https://doi.org/10.1016/j.bios.2022.114662

Rational Design and Structural Engineering of Heterogeneous Single-Atom Nanozyme for Biosensing

Ying Wang,[a] *Ruolan Du,*[a] *Lawrence Yoon Suk Lee,*[a,b,]* *Kwok-Yin Wong*[a,]*

[a] Department of Applied Biology and Chemical Technology and the State Key Laboratory of Chemical Biology and Drug Discovery, The Hong Kong Polytechnic University, Hung Hom, Kowloon, Hong Kong SAR, China

[b] Research Institute for Smart Energy, The Hong Kong Polytechnic University, Hung Hom, Kowloon, Hong Kong SAR, China

* Correspondence: lawrence.ys.lee@polyu.edu.hk; kwok-yin.wong@polyu.edu.hk

Abstract

Nanozymes, an emerging family of heterogeneous nanomaterials with enzyme-like characteristics, offer significant advantages as alternatives to natural enzymes for diverse biocatalytic applications. Nevertheless, the inhomogeneous configuration of nanomaterials makes it extremely challenging to develop nanozymes of desired performance and reaction mechanism. Single-atom nanozymes (SAzymes) that are composed of single-atomic active sites may provide an answer to these challenges with remarkable enzyme-like activity and specificity. The well-defined coordination microenvironments of SAzymes offer a suitable model system to investigate the structure–activity relationship and thus bridge the gap between natural enzyme and nanozyme. In this review, we would first present an overview of discoveries, advantages, and classifications of SAzymes. Then, we would discuss the reaction mechanism, design principles, and biosensing applications of a series of typical SAzymes with a focus on the rational design strategies for targeted reaction and the effort to uncover the catalytic mechanism at the atomic scale. Finally, we would provide the challenges and future perspectives of SAzymes as the next-generation nanozymes.

Keywords: single-atom; nanozyme; biosensing; structural engineering; heterogeneous catalysis

1. Introduction

Natural enzymes are an important class of homogeneous biocatalysts that possess excellent catalytic efficiency and high substrate specificities for multiple biological reactions in living systems (Bornscheuer et al. 2012). By exploiting the unique characteristics of natural enzymes, a number of biosensing platforms with satisfactory sensitivity and selectivity have been developed (Bell et al. 2021). In practical biosensing applications, however, the intrinsic limitations of natural enzymes, such as the restricted physiological conditions, poor stability and reusability, and complex preparation and storage processes, greatly hinder their broader clinical translation. To overcome these problems, artificial enzyme mimics have been explored as the ideal alternatives over the past few decades (Breslow 1995). In 2004, the term "nanozymes" was coined for those enzyme mimics by Pasquato and co-workers (Manea et al. 2004). Then in 2007, Yan's group first demonstrated the unexpected peroxidase (POD)-like activity of heterogeneous Fe_3O_4 nanoparticles (Gao et al. 2007). Following this intriguing work, numerous nanomaterials that possess enzyme-like properties have been reported (**Figure 1a**) (Wei and Wang 2013; Hou et al. 2019; Huang et al. 2019b; Wang et al. 2022c). Embracing the merits of natural enzymes and nanomaterials, these nanozymes can offer remarkable advantages such as high catalytic activity, stability, structural tunability, and cost-effectiveness (Jiang et al. 2019; Zhang et al. 2021a). The enzyme-like properties of nanozymes are closely related to their size dimension, morphology, exposed crystal surface, and local atomic environments (Wei and Wang 2013; Wang et al. 2020). Despite the surging number of reports on new nanozymes, there are still some major hitches that delay the development of this exciting field: (1) The inhomogeneous elemental composition and complicated nanostructures of nanozymes make it extremely challenging to precisely regulate their catalytic performance. (2) Although the nanozymes with multi-enzyme activities are advantageous for biological reactions that are often a cascade catalytic reaction, this can also severely lower their specificity. (3) The reaction mechanism of nanozymes is more complex than that of natural enzymes owing to their uncertain active sites (Yang et al. 2021). Thus, it is urgent and highly desirable to establish a rational design approach to the state-of-the-art nanozymes based on the comprehension of their structure–property relationship rather than by a trial-and-error strategy.

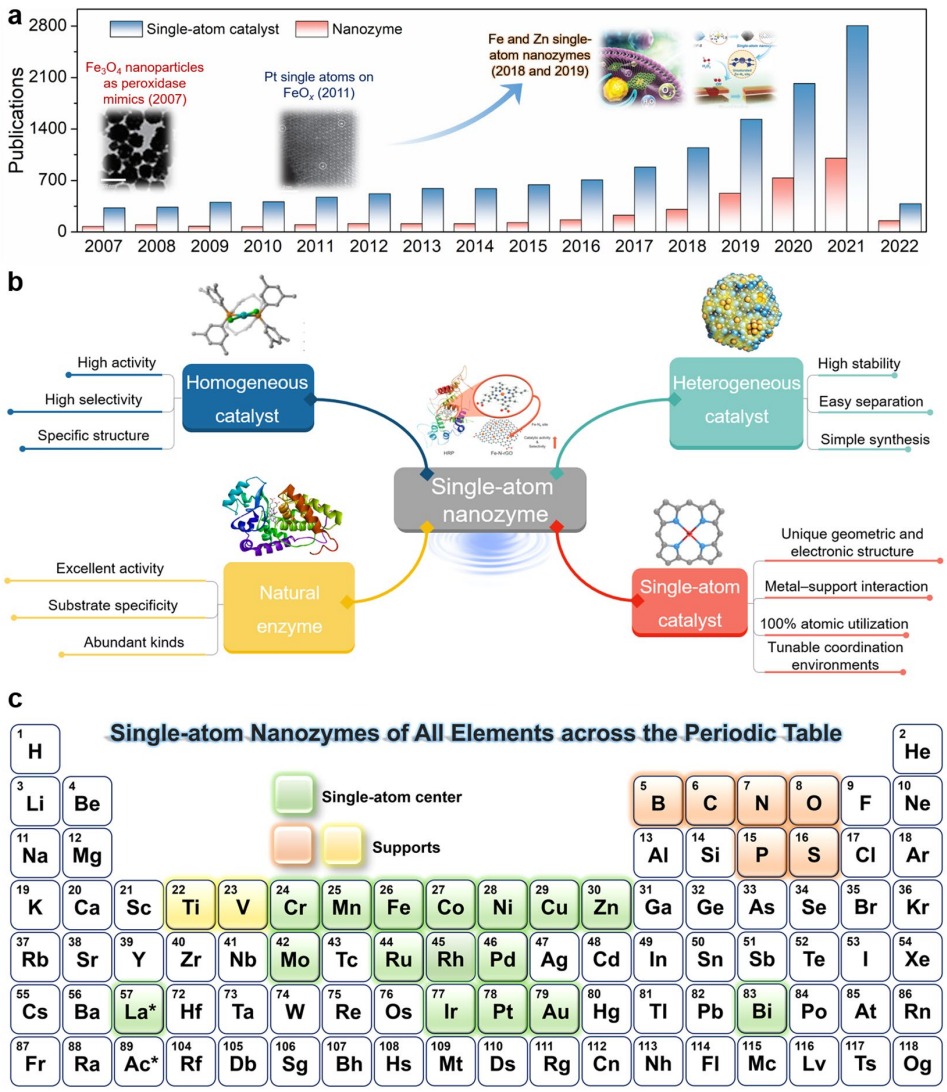

Figure 1. (a) Statistical data of the number of publications on single-atom catalysts (SACs) and nanozymes from the Web of Science from January 2007 to March 2022. Keywords: "single-atom" or "single atom catalyst"; "Nanozyme" or "enzyme-like" or ("nano" AND "enzyme-mimic") or ("nano" AND "enzyme"). Reprinted with permission from references (Gao et al. 2007; Qiao et al. 2011; Ma et al. 2019; Xu et al. 2019). (b) Overview of the SAzymes that incorporate the unique characteristics of natural enzymes, SACs, and homogeneous and heterogeneous catalysts. Reprinted with permission from references (Kim et al. 2019; Gallarati et al. 2020; Zhang et al. 2021d) (PDB entry 1W4W). (c) Schematic diagram of SAzymes of various elements across the periodic table.

Along with the rapid development of nanoscale chemistry and materials science, single-atom catalysts (SACs) have emerged as a "silver bullet" that integrates the virtues of both heterogeneous and homogeneous catalysts (Yang et al. 2013; Cui et al. 2018; Wang et al. 2018). Since the concept of SACs was first proposed by Zhang *et al*. in 2011 (**Figure 1a**) (Qiao et al. 2011), stunning development was witnessed in various catalytic reactions over the past decade (Ji et al. 2020; Kaiser et al. 2020). Various "bottom-up" and "top-down" approaches for the

synthesis of SACs were developed based on the type of precursors. The single-atom was stabilized on the supports without agglomeration by the spatial confinement, co-precipitation, atomic layer deposition, electrochemical, or photochemical strategies. Compared with traditional nanoparticles, SACs can provide maximum atom-utilization efficiency and well-defined atomic coordination, which endow them with unique advantages in establishing the structure–activity/functionality relationships to elucidate catalytic mechanisms (Li et al. 2020a; Zhang et al. 2022b). From a proof-of-concept point of view, SACs can serve as an ideal model of and promising alternatives to natural enzymes. In 2018, Mao and co-workers reported that atomically dispersed Fe atoms could serve as a highly efficient single-atom CAT and SOD mimic, which marked the first single-atom nanozymes (SAzymes, **Figure 1b**) (Ma et al. 2019). Another Zn SAzyme was also reported by Yan's group followed close behind (Xu et al. 2019). Since then, an ever-growing number of SAzymes have been designed and explored as the next generation nanozymes (Jiao et al. 2020c; Wu et al. 2020a; Chang et al. 2022). SAzymes not only achieve better enzyme-like activity and greater specificity with under-coordinated active sites but also serve as an ideal model to uncover the intrinsic catalytic mechanism at the atomic scale (Xiang et al. 2020; Wang and Zhao 2021; Wu et al. 2021). To date, abundant feasible structures of SAzymes have been fabricated with diverse transition metals (Cr, Mn, Fe, Co, Ni, Cu, Zn, Mo, Ru, Rh, Pd, Ir, Pt, and Au), post-transition metals (Bi), and lanthanum metal (Ce) as active centers (**Figure 1c**) (Pei et al. 2020). Those SAzymes demonstrated impressive characteristics of oxidoreductase mimics, including POD-like, oxidase (OXD)-like, catalase (CAT)-like, superoxide dismutase (SOD)-like, glutathione (GSH) peroxidase (GP_x)-like, and glutathione oxidase ($GSHO_x$)-like properties. These attractive enzyme-mimetic features of SAzymes have opened up a variety of application paths in the fields of biosensing, immunoassay, and reactive oxygen species (ROS) regulation-based biological applications (**Figure 2a**) (Zhang et al. 2020). Despite their extraordinary development, the activity and specificity of SAzymes are still not comparable to natural enzymes, and their ambiguous enzyme-like mechanism remains a great challenge.

The recent progress made on the synthesis and application of various SAzymes has been summarized in some review articles (Jiao et al. 2020c; Kandathil and Patil 2021), yet discussion that focuses on the rational design of SAzymes on the atomic scale, which is crucial to

understand their structure–activity relationship, is not yet available. Thus, it is important and timely to make a critical review on the recent development of the precise fabrication of SAzymes and the uncovering of their intrinsic catalytic mechanisms to gain a deeper insight into the origin of their enzyme-like properties. In this review, a series of typical SAzymes would be classified based on their inherent enzyme-like properties (**Table 1**). Then, we would provide a comprehensive review of the different strategies for rational design and microenvironment tuning of targeted SAzymes (**Figure 2b**). In particular, the inherent enzyme-like activity, specificity, and stability of SAzymes would be elaborated from the perspectives of structural engineering and electronic modulation. The impressive advancements of SAzymes as innovative analytical platforms in biosensing applications would be also highlighted. Last but not least, the remaining challenges of SAzymes would be pointed out with future perspectives and opportunities for the further development of SAzymes.

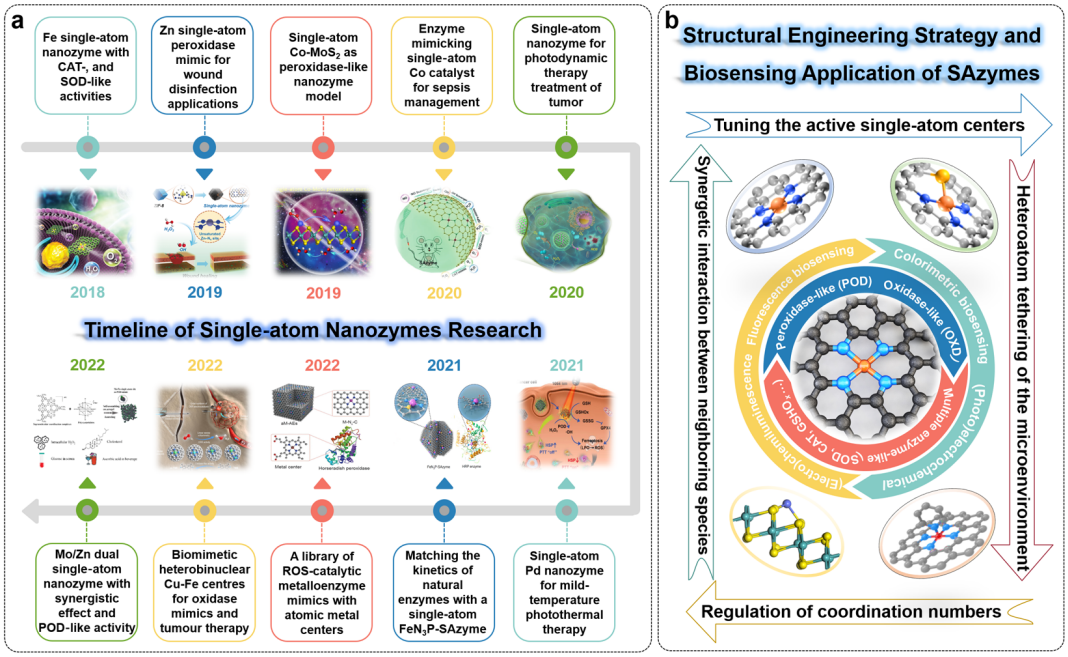

Figure 2. (a) A brief timeline for the development of SAzymes (SAzyme). OXD, oxidase; POD, peroxidase; SOD, superoxide dismutase; CAT, catalase; C.N., coordination number; ROS, reactive oxygen species. Reprinted with permission from reference (Ma et al. 2019; Wang et al. 2019c; Xu et al. 2019; Cao et al. 2020; Chang et al. 2021; Ji et al. 2021; Wang et al. 2021a; Wang et al. 2021d; Cao et al. 2022; Lu et al. 2022). (b) Illustration of structural engineering strategy and biosensing application of SAzymes.

Table 1. (a) A summary of representative SAzymes for diverse biological applications.

SAzyme	Active site	Mimic function	Application	Reference
Fe–N–C	$Fe–N_4$	POD	Colorimetric biosensing of H_2O_2	(Jiao et al. 2020a)
Fe–N-rGO	Fe	POD	Colorimetric biosensing of H_2O_2 and acetylcholine	(Kim et al. 2019)
IIM-Fe-SASC	Fe	POD	Colorimetric biosensing of H_2O_2	(Lyu et al. 2021)
FeN_5	$Fe–N_5$	POD	Tumor catalytic therapy	(Xu et al. 2022)
$Fe_{SA}–Pt_C$	Fe sites + Pt_C	POD	Colorimetric biosensing of PSA	(Chen et al. 2021a)
Cu SASs/NPC	$Cu–N_4$	POD	Photothermal therapy	(Wang et al. 2021c)
PMCS	$Zn–N_4$	POD	Wound disinfection	(Xu et al. 2019)
NO_2-MIL-101	$Fe–N_5$	POD	Colorimetric biosensing of AChE	(Xu et al. 2020)
FeBNC	$Fe–N_4B_1$	POD	Colorimetric biosensing of AChE and OPs	(Jiao et al. 2020b)
FeSNC	$Fe–N_3S_1$	POD	Colorimetric biosensing of OPs	(Jiao et al. 2021)
FeN_3P	FeN_3P	POD	Inhibition for tumor cell growth	(Ji et al. 2021)
Pt_{TS}-SAzyme	Pt_1-N_3PS	POD	Antibacterial application	(Chen et al. 2021b)
ZnBNC	$Zn–BN_4$	POD	Colorimetric biosensing of *p*-phenylenediamine	(Feng et al. 2022)
SA Co-MoS_2	SA-Co	POD	Colorimetric and electrochemical biosensing of H_2O_2	(Wang et al. 2019c)
$(Fe,Pt)_{SA}$-N-C	$Fe–N_3/Pt–N_4$	POD	Tumor catalytic therapy	(Wang et al. 2022a)
Zn/Mo DSAC-SMA	Zn/Mo sites	POD	Colorimetric biosensing of H_2O_2, glucose, cholesterol, and AA	(Ma et al. 2022)
Fe_3C@C/Fe–N–C	$Fe–N_4$+Fe_3C clusters	POD	Electrochemical biosensing of H_2O_2	(Wei et al. 2021)
Mo_{SA}-N_x-C	$Mo–N_3$	POD	Colorimetric detection of H_2O_2 and xanthine	(Wang et al. 2021d)
Cu–N–C	$Cu–N_4$	POD	Colorimetric biosensing of AChE activity and OPs	(Wu et al. 2020b)
Ce–N–C	$Ce–N_4$	POD	Colorimetric biosensing of pesticide residues	(Song et al. 2022)
FeSAC/Cu_2O/$Ti_3C_2T_x$	Fe	POD	Photoelectrochemical biosensing of AChE activity and OPs	(Qin et al. 2022)
Fe_2NC	Fe_2 sites	OXD	Colorimetric biosensing of S^{2-}	(Jiao et al. 2022)
Fe–N/C-CNTs	$Fe–N_3$	OXD	Colorimetric biosensing of GSH	(Wang et al. 2019d)
FeN_5 SA/CNF	$Fe–N_5$	OXD	Antibacterial application	(Huang et al. 2019a)
Cu/Fe-DACs	Cu/Fe	OXD	Tumour therapy	(Lu et al. 2022)
Pd SAzyme	$Pd–N_4$	OXD	Colorimetric biosensing of antioxidant capacity	(Li et al. 2022c)
Fe–N–C	$Fe–N_4$	OXD	Colorimetric biosensing of AA	(Shen et al. 2022)
Cu-SAzyme	$Cu–N_4$	SOD	Treatment of sepsis	(Yang et al. 2022)
Fe-SAs/NC	$Fe–N_4$	SOD, CAT	Oxidative stress cytoprotection	(Ma et al. 2019)

SAzyme	Active site	Mimic function	Application	Reference
Co/PMCS	Co–N_4	SOD, CAT, GP_x	Sepsis management	(Cao et al. 2020)
Mn/PSAE	Mn–N_3	POD, OXD, CAT	Photothermal therapy	(Zhu et al. 2021)
Ru SAEs	Ru	$GSHO_x$, OXD, POD	Cancer therapy	(Wang et al. 2021b)
Pt/CeO_2	Pt	POD, CAT, SOD, GP_x	Non-invasive treatment of neurotrauma	(Yan et al. 2019)
pero-nanozysome	Fe–N_4+Fe clusters	POD, OXD, CAT, SOD, UOD	Hyperuricemia treatment and the protection of neurons	(Xi et al. 2021)
Pd SAzyme	Pd–N_4 sites	POD, $GSHO_x$	Mild-temperature photothermal therapy	(Chang et al. 2021)

2. Enzymatic Activities and Mechanisms of SAzymes

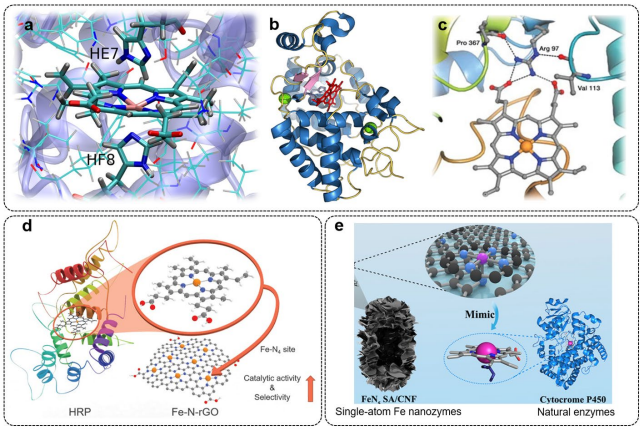

Figure 3. Crystal structure of (a) oxymyoglobin (Bringas et al. 2017), (b) horseradish peroxidase (Krainer and Glieder 2015), and (c) cytochrome P450 proteins (CYP2C9) (Williams et al. 2003). (d) A comparison between the cofactor structure of HRP and the Fe–N_4 site embedded in graphene (Kim et al. 2019). (e) Schematic illustration of the structural similarity between FeN_5 SA/CNF SAzyme and iron-heme groups in cytochrome P450 (Huang et al. 2019a). Reprinted with permission from reference.

Naturally occurring enzymes are considered homogeneous biocatalysts, but the active sites of enzymes, such as the dual-Ni species in urease, single-Mo–N_4 moieties in nitrogenase (Wang et al. 2019b), and single-Mg–N_4 centers in chlorophyll, resemble the single-atomic metal active centers of heterogeneous SACs. Such intriguing structural similarities have inspired the development of SACs for heterogeneous catalysis of the corresponding target reactions. In particular, the single Fe cofactor connected by a proximal ligand in representative heme proteins (*e.g.*, oxymyoglobin, horseradish peroxidase, and cytochrome P450 proteins) is

similar to the SAzymes with built-in Fe–N_x active sites (**Figure 3a–3c**) (Huang et al. 2019a; Kim et al. 2019). In this section, various enzymatic activities of bioinspired SAzymes and their underlying mechanisms in mimicking the geometric and chemical structure of natural enzymes would be discussed.

2.1. POD-Like Activity

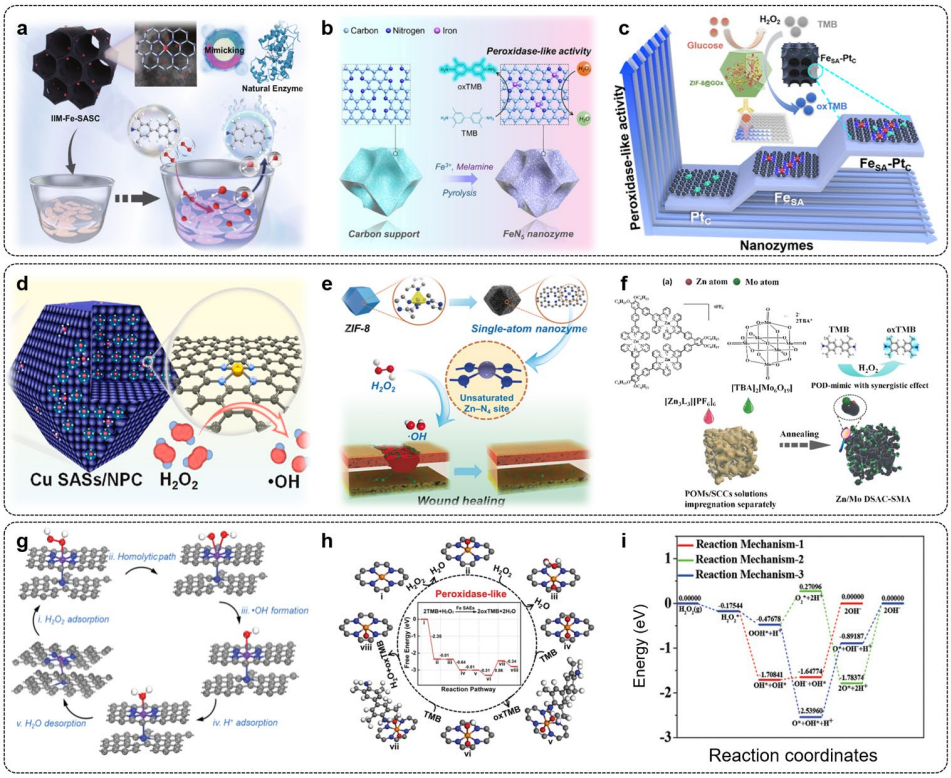

Figure 4. (a) Isolated Fe–N–C single-atomic site catalysts (IIM-Fe-SASC) with POD-like activity toward the detection of hydrogen peroxide (Lyu et al. 2021). (b) Bioinspired Fe single-atom POD-like nanozymes with five-coordinated structure (FeN_5 SAzyme) (Lu et al. 2022). (c) Fe–N–C SACs coupled with Pt clusters (Fe_{SA}-Pt_C) as highly active POD-like nanozymes (Chen et al. 2021a). (d) Cu single-atom sites anchored on N-doped porous carbon (Cu SASs/NPC) (Wang et al. 2021c). (e) Atomically dispersed Zn-centered atoms derived from zeolitic imidazolate frameworks (ZIF-8) as single-atom POD mimics (Xu et al. 2019). (f) Dual atomic SAzymes with Zn/Mo dual-atom sites (Ma et al. 2022). (g) Proposed catalytic principle of POD-like reaction on FeN_5 SAzymes (Lu et al. 2022). (h) Proposed reaction pathways with the corresponding intermediates of POD-like activity of Fe SAEs (Wang et al. 2019b). (i) Energy diagram of the proposed POD-like reaction process for decomposing H_2O_2 by hemolytic and heterolytic paths on Fe–N–C models (Xu et al. 2021). Reprinted with permission from references.

Horseradish peroxidase (HRP) is a typical peroxidase that can catalyze the oxidation of substrates using H_2O_2 as an electron acceptor (Berglund et al. 2002). Inspired by the active Fe-centered heme species in HRP, several SACs have been designed to serve as artificial enzymes with comparable POD-like activity and selectivity. Zhu and colleagues proposed a universal

salt-template strategy for synthesizing ultrathin sheet-like single-atom Fe–N–C nanozymes (Jiao et al. 2020a). These SAzymes containing dense isolated Fe–N_4 sites exhibited promising POD-like activities owing to their structures similar to natural HRP. Guided by this strategy, Lee and coworkers adopted the Fe–N_4 single site-embedded graphene (Fe-N-rGO) to imitate the heme-cofactor structure of natural HRP (**Figure 3d**) (Kim et al. 2019). The as-synthesized Fe-N-rGO SAzyme possessed intrinsic POD-like catalytic features that were superior to those of undoped rGO and commercial Fe_3O_4 nanoparticles. Lyu and coworkers fabricated another typical isolated Fe–N–C single-atomic site catalyst (IIM-Fe-SASC) by a facile ion-imprinting method, which showed boosted POD-like activity (**Figure 4a**) (Lyu et al. 2021). The resultant IIM-Fe-SASC could serve as an ideal nanoprobe to achieve selective detection of H_2O_2. Very recently, Liu and coworkers successfully fabricated Fe-based SAzymes that were composed of Fe single atoms coordinated by five N atoms (FeN_5) *via* a melamine-mediated pyrolysis activation strategy (**Figure 4b**) (Lu et al. 2022). The as-fabricated FeN_5 SAzymes exhibited superior POD-like activity and catalytic efficiency, which was *ca*. 7.64 and 3.45 × 10^5 times higher than that of traditional FeN_4 SAzymes and Fe_3O_4 nanozymes, respectively. Both experimental and theoretical investigations revealed that the bioinspired atomically dispersed Fe–N_5 moieties could promote the activation of H_2O_2 substrates and charge transfer, thus achieving enhanced POD-like activity. Zhu and coworkers reported another design strategy for Fe-based SAzymes, which involved the coupling of Pt clusters with Fe–N–C SACs (**Figure 4c**) (Chen et al. 2021a). The as-proposed Fe_{SA}–Pt_C nanozyme exhibited enhanced POD-mimicking activity thanks to the synergistic effect between the atomically dispersed Fe–N–C support and Pt clusters.

More SACs based on transition metals other than Fe were also reported to possess POD-like properties. Cheng's group designed and synthesized Cu single-atom sites on N-doped porous carbon support (Cu SASs/NPC) by pyrolysis–etching–adsorption–pyrolysis method (**Figure 4d**) (Wang et al. 2021c). The obtained Cu SASs/NPC possessed POD-like catalytic activity to efficiently generate abundant •OH species in the presence of H_2O_2 substrates. Another interesting example of Zn-based SAzymes was presented by Yan and coworkers (Xu et al. 2019). They engaged ZIF-8-derived Zn–N–C SACs to construct a Zn-centered porphyrin-like structure (PMCS, **Figure 4e**). These PMCS SAzymes with atomically dispersed and

unsaturated single Zn atoms (Zn–N_4) exhibited comparable POD-like performance and significantly facilitated wound healing with a high therapeutic effect.

Numerous natural enzymes contain binuclear active centers equipped with multiple coenzymes and/or cofactors (Baddiley et al. 1953). Wei and coworkers designed a Zn/Mo dual-atomic SAzyme anchored on macroscopic aerogel (Zn/Mo DSAC-SMA) as a proof-of-concept model (**Figure 4f**) (Ma et al. 2022). The Mo site possessed a stronger affinity to hydroxyl species than the Zn site, thus the oxidation of TMB substrates was more likely to occur on the Zn site with a small energy barrier. Such Zn/Mo dual site was readily identified as the main active center that displayed remarkable POD-like activity. The well-defined and uniform configurations of active sites in those SAzymes enabled the investigations of the underlying POD-like reaction mechanism on the atomic level. Shi and colleagues reported the acidity-accelerated heterogeneous catalytic Fenton reaction on single-atom Fe-containing POD-like SAzymes (PSAF NCs) (Huo et al. 2019). First, H_2O_2 molecules were split into two hydroxyl group species (*OH and •OH) by a homolytic path at the active Fe–N_4 center. Then, the protonation of *OH under acidic conditions produced surface-adsorbed water molecules that regenerated the surface upon subsequent desorption. In contrast, *OH species would lead to the poisoning of Fe–N_4 active sites under neutral conditions. Therefore, the POD-like reaction kinetics and radical-generating characteristics of these PSAF NCs were attributed to the difference between the acidic and neutral conditions. In another study by Fan and coworkers, an experimental model with an Fe–N_5 active center was built to explore the POD process (Lu et al. 2022). As illustrated in **Figure 4g**, the H_2O_2 adsorption was the first elementary step with a high affinity of FeN_5 SAzyme towards H_2O_2. These activated H_2O_2 molecules were split into two surface-adsorbed hydroxyl species (*OH) by a homolytic path, followed by the desorption of one *OH to form an active hydroxyl radical (•OH). The FeN_5–OH structures returned to their initial state with the desorption of the H_2O molecules under acidic conditions. It is worth noting that the typical 3,3′,5,5′-tetramethylbenzidine (TMB) substrate could also participate in the POD-like catalytic process by transferring electron to SAzymes. A more comprehensive investigation of the whole POD-like pathways was undertaken by considering both the decomposition of H_2O_2 and electron–proton pair transfer (**Figure 4h**) (Wang et al. 2019b). To be specific, the H_2O_2 molecules could spontaneously dissociate into O* intermediates on the

optimized Fe–N_4 moieties by a heterolytic path. Accordingly, O=Fe=O structure was formed on the central Fe–N_4 moiety with the dissociation of another H_2O_2 molecule. Meanwhile, the free-energy profiles for the POD-like reaction were accompanied by electron transfers from the oxidization of TMB ($_{ox}$TMB) and proton transfers from the acidic medium. All electron-transfer steps were thermodynamically favorable with the decomposition of H_2O_2 to form $_{ox}$TMB and H_2O on the surface of FeN_4 SAzymes. To further elucidate the dissociation of H_2O_2* *via* a homolytic or heterolytic pathway, the corresponding reaction energy levels were evaluated by density functional theory (DFT) calculations (Xu et al. 2021). Compared with the heterolytic pathway for the H_2O_2* to O* + H_2O*, the homolytic pathway for the H_2O_2* to 2OH* was kinetically more favorable on the central single Fe active site of Fe–N–C POD-like SAzymes (**Figure 4i**). To summarize, those single-atom active sites in SAzymes play an important role in improving the POD-like activity from both experimental and theoretical perspectives (**Table 2**).

Table 2. Comparison of apparent Michaelis-Menten constant (K_m), maximum reaction rate (V_{max}), catalytic constant (k_{cat}), and specific activity (SA) of various SAzymes as peroxidase mimetics.

SAzyme	Substance	K_m [mM]	V_{max} [$\times 10^{-7}$ M·s^{-1}]	k_{cat} [s^{-1}]	SA [U mg^{-1}]	Reference
Fe–N–C	TMB	5.20	14.90	-	25.33	(Jiao et al. 2020a)
	H_2O_2	4.31	6.20	-		
Fe–N-rGO	TMB	0.074	17.4	1.45×10^5	-	(Kim et al. 2019)
	H_2O_2	43	14.4	1.20×10^5		
IIM-Fe-SASC	TMB	48.45	8.08	3.62×10^3	48.5	(Lyu et al. 2021)
	H_2O_2	5.65	0.94	4.15×10^3		
FeN_5	TMB	0.652	84.7	3.92	-	(Xu et al. 2022)
	H_2O_2	11.2	29.6	1.37		
FeN_4	TMB	0.577	15.7	0.633		
	H_2O_2	15.6	6.18	0.249		
Fe_{SA}–Pt_C	TMB	1.8	14.0	-	87.7	(Chen et al. 2021a)
	H_2O_2	19.6	16.0	-		
PMCS	TMB	0.224	1.066	4.97×10^6	-	(Xu et al. 2019)
	H_2O_2	40.16	1.215	5.66×10^6		
Zn/Mo DSAC-SMA	TMB	0.43	0.384	0.081 (Zn) 0.026 (Mo)	-	(Ma et al. 2022)
	H_2O_2	40.32	3.33	0.705 (Zn) 0.219 (Mo)		
NO_2-MIL-101	TMB	9.01	15.03	-	35.70	(Xu et al. 2020)

Ru SAEs	H_2O_2	1.10	8.89	-	7.5	(Wang et al. 2021b)
	TMB	0.22	11	-		
	H_2O_2	0.085	6.9	-		
FeBNC	TMB	2.22	18.1	0.52	15.41	(Jiao et al. 2020b)
	H_2O_2	25.24	12.8	0.37		
FeSNC	TMB	2.46	20.1	-	79.71	(Jiao et al. 2021)
	H_2O_2	25.44	26.1	-		
FeN_3P	TMB	206	465	4.82	316	(Ji et al. 2021)
	H_2O_2	443	336	5.28		
Pt_{TS}-SAzyme	TMB	0.31	2.83	329	21.8	(Chen et al. 2021b)
ZnBNC	TMB	0.11	1.09	-	-	(Feng et al. 2022)
	H_2O_2	1.24	1.12	-		
Cu–N–C	TMB	3.76	7.51	0.28	-	(Wu et al. 2020b)
	H_2O_2	19.94	2.01	0.075		
Mo_{SA}-N_3-C	TMB	0.79	1.12	0.06	-	(Wang et al. 2021d)
	H_2O_2	2.00	3.7	0.20		
Fe SAEs	TMB	3.92	5.88	0.55	-	(Zhao et al. 2019)
	H_2O_2	0.243	0.825	0.077		
Mn/PSAE	TMB	0.14	3.0	1.36×10^5	-	(Zhu et al. 2021)
	H_2O_2	0.09	1.6	7.7×10^4		
Fe_2NC	TMB	1.36	6.61	-	-	(Jiao et al. 2022)
	H_2O_2	31.89	7.27	-		
HRP	TMB	0.434	1.0	-	-	(Gao et al. 2007)
	H_2O_2	3.702	0.871	-		

2.2. OXD-Like Activity

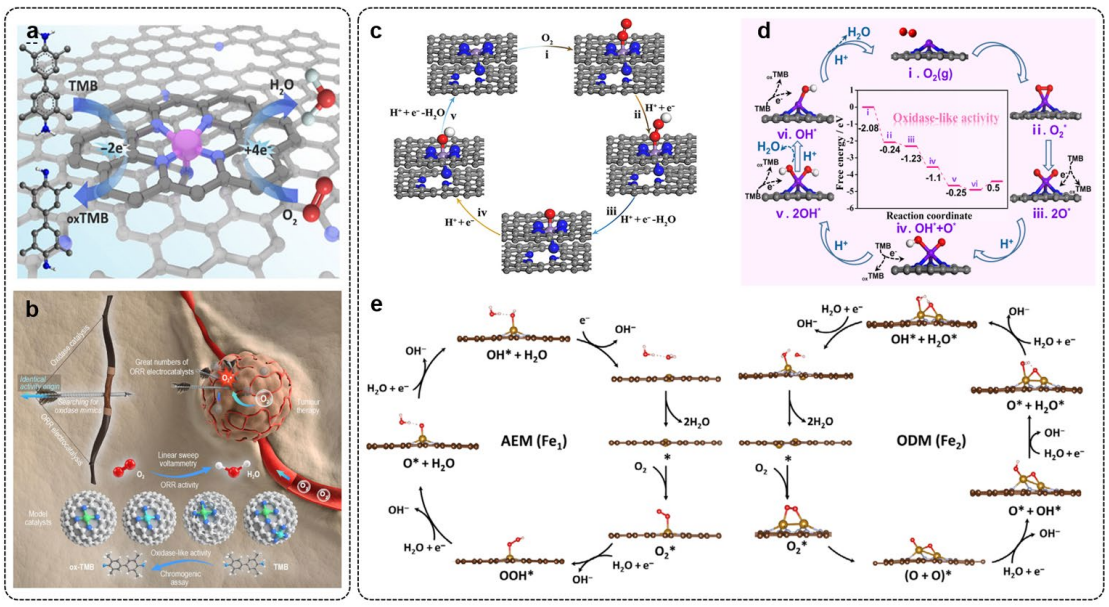

Figure 5. Schematic diagrams of (a) single-atom OXD mimic with the carbon nanoframe-confined Fe–N_5 active sites (FeN_5 SA/CNF) (Huang et al. 2019a) and (b) OXD-like catalysis by Cu/Fe-doped SACs (Lu et al. 2022). (c) Proposed mechanism of the OXD-like reaction with the optimized adsorption configurations

on FeN_5 SA/CNF (Huang et al. 2019a). (d) Theoretical investigation and optimized geometric structures of the proposed OXD-like reaction process on the Fe-N/C-CNTs (Wang et al. 2019d). (e) The corresponding schematic diagram of the *peroxo*-like O_2 adsorption on Fe_1NC (single-atom Fe on N-doped porous carbon) and Fe_2NC *via* ODM and AEM pathways (Jiao et al. 2022). Reprinted with permission from references.

Despite the considerable development made in the POD-like SAzymes, there are still several problems in their biological application, especially the heavy reliance on H_2O_2 substrates. Unlike POD-like nanozymes, oxidases (OXD) can activate molecular O_2 to yield ROS without the additional demands of H_2O_2 (Chong et al. 2021). In this context, Fe–N–C SAzyme with high surface area and abundant defect sites was developed by a general ionic salt-assisted synthetic method (Shen et al. 2022). This KCl-treated Fe–N–C SAzyme displayed remarkable OXD-mimicking activity that surpassed NaCl-treated Fe–N–C and typical Fe_3O_4 nanozymes. In addition to the $Fe–N_4$ configurated Fe–N–C SAzymes, Dong and coworkers also constructed a carbon nanoframe-confined axial FeN_5 SAzyme (FeN_5 SA/CNF) using a bottom-up strategy (**Figure 5a**) (Huang et al. 2019a). The as-designed FeN_5 SA/CNF exhibited a higher OXD-like activity than MnN_5 SA/CNF, CoN_5 SA/CNF, NiN_5 SA/CNF, CuN_5 SA/CNF, and FeN_4 SA/CNF. More encouragingly, the axial $Fe–N_5$ structure of this SAzyme, which resembled the ligand-coordinated heme of cytochrome P450, endowed unique electron push and synergistic effects to achieve significantly enhanced OXD-like activity. Very recently, Lu *et al*. fabricated Pd SACs anchored on N-doped carbon supports (SA Pd/NC) with maximum atom utilization *via* a general host–guest approach (Xu et al. 2022). The introduction of well-established $Pd–N_4$ units successfully enhanced the OXD-like catalytic performance.

Recently, binuclear SAzymes built by introducing a secondary metal site have drawn attention as a closer mimic of natural enzymes. Zhu and coworkers constructed an atomically dispersed Fe–Fe dimer as a coordination center embedded in the metal–organic frameworks (MOF)-derived N-doped carbon (Fe_2NC) (Jiao et al. 2022). The Fe_2NC dual-atom nanozyme served as a proof-of-concept model imitating the cytochrome *c* oxidase (CcO). Compared with single-atomic Fe_1NC SAzymes, Fe_2NC dual-atom nanozyme could better activate oxygen molecules and thus achieved enhanced enzyme-like activities by the cooperative interactions between neighboring Fe atoms. Shi and colleagues took one step further to more precisely reproduce the active site of CcO, which contained Cu atoms as the electron donor in the vicinity of Fe active site (Lu et al. 2022). They designed Cu/Fe-doped SACs with biomimetic

heterobinuclear Cu–Fe centers (**Figure 5b**). The Cu atom improved the protonation of O_2 species and the desorption of H_2O products on the Fe sites. Therefore, the Cu–Fe dual-atoms effectively boosted the OXD-like activity with enhanced electrocatalytic oxygen reduction reaction (ORR) activity. The activities of these OXD-like SAzymes are quantitatively compared in terms of typical kinetic constants and summarized in **Table 3**.

Table 3. Comparison of apparent K_m, V_{max}, k_{cat}, and SA of various SAzymes as oxidase mimetics (taking TMB as the substrate).

SAzyme	K_m [mM]	V_{max} [$\times 10^{-7}$ M·s^{-1}]	k_{cat} [s^{-1}]	SA [U mg^{-1}]	Reference
FeN_5 SA/CNF	0.148	7.58	0.71	-	(Huang et al. 2019a)
Cu/Fe DACs	0.21	2.8	0.0845	89.86	(Lu et al. 2022)
Fe SAEs	0.13	0.225	0.021	-	(Zhao et al. 2019)
Pd SAzyme	0.056	2.38	2.5×10^6	-	(Li et al. 2022c)

The OXD-like reaction mechanism shares similarities with the ORR *via* the adsorption evolution mechanism (AEM). Dong *et al.* employed theoretical calculations to explore the intrinsic OXD-like activity on an Fe–N_4 site in a graphene matrix coupled with pyridinic N *via* a direct 4e$^-$ reduction pathway (**Figure 5c**) (Huang et al. 2019a). They showed that O_2 could be spontaneously chemisorbed on the surface of FeN_5 SA/CNF *via* an end-on configuration with elongated O–O bonds. The distance of the O–O bond in the adsorbed *O_2 species was much longer on FeN_5 SA/CNF than on MnN_5 SA/CNF, CoN_5 SA/CNF, and FeN_4 SA/CNF. By virtue of the strong electron push effect, the activated O_2 was more likely to acquire acidic hydrogens to form surface-adsorbed *OOH species. Such a unique configuration of FeN_5 SA/CNF could optimize the whole OXD-like reaction pathway.

Recently, Cui and coworkers fabricated single-atomic Fe–N_3 moiety embellished N-doped carbon supports (Fe-N/C-CNTs) as an OXD-like paradigm (Wang et al. 2019d). The OXD-like reaction process of Fe-N/C-CNTs was shown to follow the proposed oxygen dissociation mechanism (ODM), which was illustrated by the following six thermochemical reaction steps (**Figure 5d**): (i–ii) The chemisorbed oxygen molecule on the surface of Fe–N_3 centers split into two separated O* atoms by the homolytic way; (ii–v) Those two dissociated O* species were

hydrogenated to form two OH* species by the electron–proton pair transfer; (v–vi) The subsequent formation and desorption of the two H_2O* species proceeded with low limiting barriers. The corresponding calculated charge density distribution for the model of adsorbed O_2 on Fe–N_3 centers also confirmed the strong charge interactions. To further elucidate these two kinds of OXD-like catalytical mechanisms, Zhu *et al*. explored the corresponding energy profile of the Fe_1NC and Fe_2NC models (**Figure 5e**) (Jiao et al. 2022). Compared with the Fe_1NC OXD mimic following the AEM process, the adsorbed O_2 molecules were more thermodynamically favorable to dissociate directly into two OH* species *via* the ODM pathway. More importantly, the O_2 dissociation energy for Fe_2NC site *via* ODM required a much smaller energy input than that *via* AEM on Fe_1NC.

2.3. Multiple Enzyme-Like Activities

In addition to the particular enzyme-like property of SAzymes, the advanced SAzymes with multiple enzyme-like catalytic activities also hold great promise in biological cascade catalytic reactions. In this regard, a class of SACs, especially the Fe-based SAzymes, was explored as potential biomimetic cascade nanoreactors. One recent study by Li *et al*. reported a single-atom Fe–N_4 catalytic site anchored on N-doped porous carbon (Fe-SAs/NC) as a bifunctional SAzyme (**Figure 6a**) (Ma et al. 2019). This antioxidative Fe-SAs/NC could mimic the catalase (CAT)-like and superoxide dismutase (SOD)-like properties to efficiently scavenge ROS for oxidative stress cytoprotection. Similarly, an atomic-level engineered Fe single-atom doped carbon dots (Fe-CDs) was prepared by microwave-assisted pyrolysis (Muhammad et al. 2022). The as-prepared Fe-CDs could mimic the activities of multiple enzymes, including SOD, CAT, GP_x, and thiol peroxidase (TP_x) under physiological conditions. The Fe-CDs also displayed OXD- and POD-like properties under acidic conditions (**Figure 6b**). This Fe-CDs SAzyme provided a potential nanoplatform in malignant glioblastoma therapy.

Dual-atom nanozymes, an emerging frontier of nanozymes, also mimic multiple enzyme-mimicking activities thanks to the unique synergistic effect. A dual-Fe-atom nanozyme (Fe_2NC) was successfully fabricated by encapsulating two neighboring Fe single-atoms into the shell layer a Se-containing MOF (Se-MOF, **Figure 6c**) (Tian et al. 2022). Compared with the single-atom Fe nanozyme (Fe_1NC), the dual-atomic Fe_2NC SAzyme exhibited markedly enhanced

OXD-like, SOD-like, and CAT-like performances. The Fe_2NC SAzyme could also effectively counteract oxidative damage to protect brain tissues. DFT calculations explained that there was a stronger synergistic effect in the Fe_2NC system than in Fe_1NC because of the simplified rearrangement structure and lower energy differences for the rate-determining step (**Figures 6d** and **6e**).

Single-atom Co-porphyrin centers supported on N-doped carbon matrixes (Co/PMCS) were also successfully synthesized to mimic multiple antioxidative enzymes (Cao et al. 2020). The Co/PMCS with CAT-like, SOD-like, GP_x-like, •OH-scavenging, and •NO-scavenging properties was further used as a promising biocompatible antioxidant. More recently, Zhu and colleagues reported that a PEGylated Mn-based SAzyme (Mn/PSAE) could be an ideal candidate for tumor therapy (**Figure 6f**) (Zhu et al. 2021). The Mn/PSAE was proved to possess multiple enzyme-like properties, such as POD, OXD, and CAT mimic enzymes, which enabled the synergetic cascade reactions. In addition to these transition metal-based SAzymes, various types of noble-metal-based SAzymes with multiple enzyme-like characteristics were also reported. For example, Ru SAzyme was carried by biocompatible carbon dots (Ru SAEs) to achieve intriguing GSH oxidase ($GSHO_x$)-, OXD-, and POD-like properties (Wang et al. 2021b). The well-established Ru SAEs with multi-enzyme-mimicking activities were further utilized for high-efficiency cascade enzyme-mimicking therapy. Lin's group fabricated a Pd SAzyme with both POD and $GSHO_x$ mimic enzyme activities using a "top-down" strategy (Chang et al. 2021). It was generally accepted that the intrinsic POD-like activity proceeded *via* the heterogeneous catalytic Fenton reaction mechanism. As for the $GSHO_x$-like activity, the GSH molecules could spontaneously form an adsorbed state on the $Pd–N_4$ active sites (**Figure 6g**). In the meantime, the reactive OH and O species from the POD-like reaction or H_2O molecules directly interacted with the absorbed GSH* to accelerate their dissociation. Consequently, the generated GS* species could couple with each other to form the GS–SG over a low energy barrier.

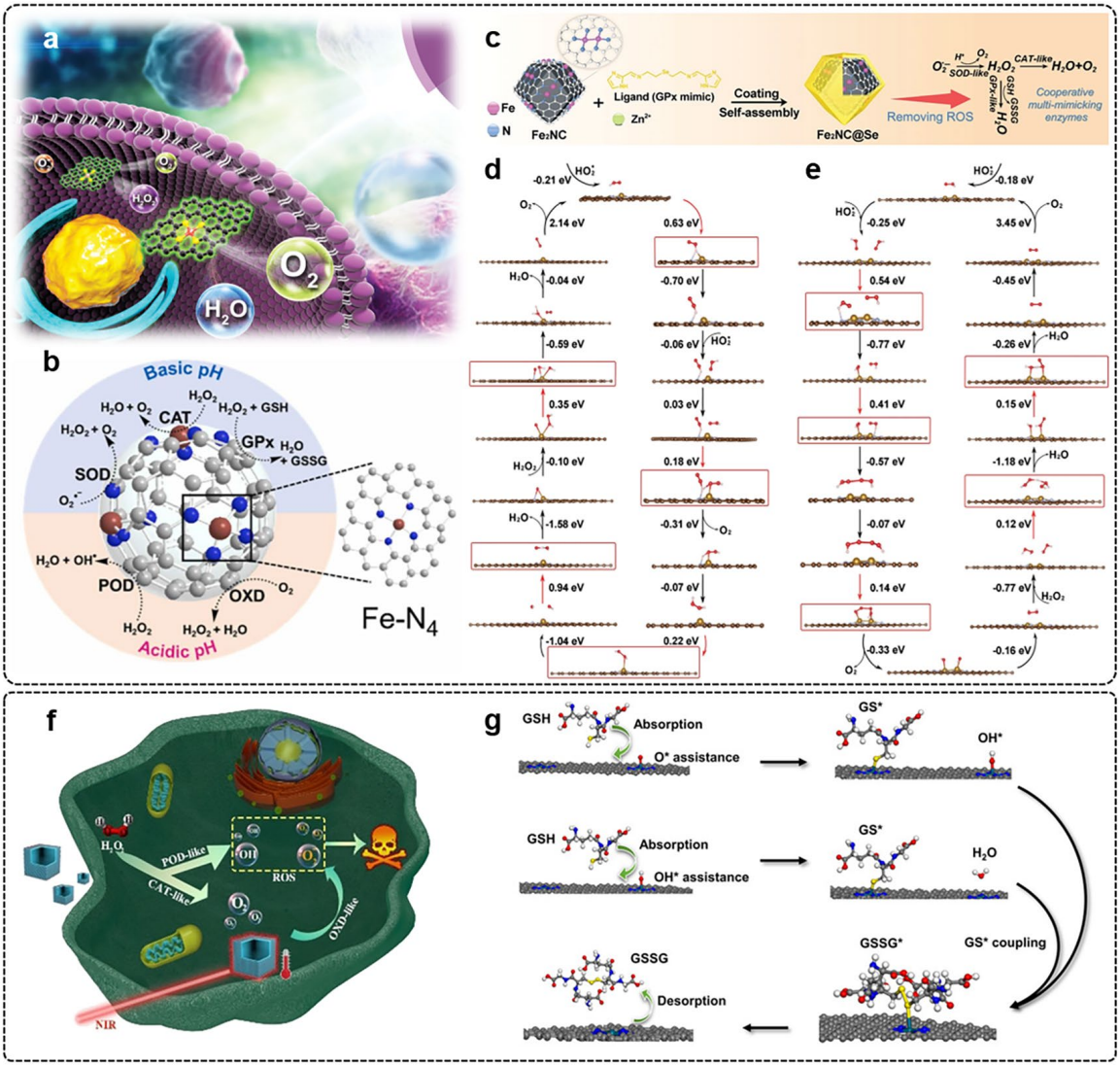

Figure 6. Schematic illustrations of (a) single-atom Fe–N_4 catalytic site anchored on N-doped porous carbon (Fe-SAs/NC) mimicking two antioxidative enzymes (Ma et al. 2019). (b) Carbon dots-supported Fe single-atom nanozyme (Fe-CDs) with the activities of six naturally occurring enzymes (OXD, CAT, SOD, POD, GP_x, and TP_x) (Muhammad et al. 2022). (c) Dual-Fe-atom nanozyme (Fe_2NC) in a Se-containing MOF (Fe_2NC@Se) with multi-enzyme mimicking activities. The free energy diagrams of CAT-like and SOD-like cascade catalytic reaction pathways with optimized adsorption configurations on (d) Fe_1NC and (e) Fe_2NC (Tian et al. 2022). (f) Schematic illustration of Mn SAzymes with POD, OXD, and CAT mimic enzyme activities (Zhu et al. 2021). (g) Proposed reaction mechanism of Pd SAzyme with $GSHO_x$-mimicking activity (Chang et al. 2021). Reprinted with permission from references.

3. Engineering Strategies for Designing Targeted SAzymes

As discussed earlier, SAzymes can serve as a kind of heterogeneous biocatalysts, and their enzyme-like catalytic activity largely relies on the physical and chemical properties of single-atomic sites. In addition to factors such as morphology, size, composition, and surface modification, the local microenvironment is also essential in regulating the enzyme-like

performance of SAzymes. However, many SAzymes are still being developed in a trial-and-error manner without comprehensive understanding or systematic guidance at the atomic level. It is of great value to know how to rationally design targeted SAzymes with satisfactory activity and specificity under the guidance of the structure–property relationship. In this section, various strategies to modulate the distinctive properties of desirable SAzymes, including tuning the active single-atom centers, heteroatom tethering, regulation of coordination numbers over single atom sites, and synergetic interaction between neighboring species, would be discussed. The associated mechanisms for the corresponding enzyme-like behaviors would be further explored based on the well-defined configuration of SAzymes.

3.1. Tuning of Active Single-Atom Centers

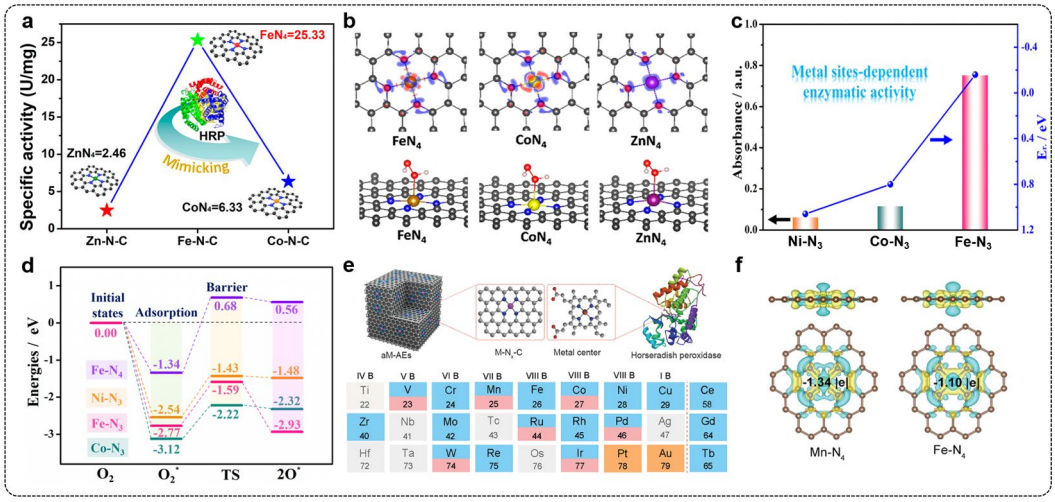

Figure 7. (a) Specific activities of different M–N_4–C SAzymes (M = Fe, Co, and Zn). (b) Calculated charge density differences and optimized geometric structures for the adsorption of H_2O_2 on M–N–C models. Red and blue areas represent the electron accumulation and electron depletion, respectively (Jiao et al. 2020a). (c) Absorbance changes of $_{ox}$TMB at 652 nm catalyzed by different M–N–C samples. (d) Energy diagram of the proposed OXD-like reaction process for M–N–C structures (Wang et al. 2019d). (e) Schematic diagram of a library of well-defined promising artificial metalloenzymes (AMEs) containing 20 different kinds of metal–N-coordinated centers with a summary of elements used in the as-synthesized AMEs. (f) Charge density differences of Fe–N_4 and Mn–N_4 sites. Cyan and yellow areas indicate charge depletion and accumulation, respectively (Cao et al. 2022). Reprinted with permission from references.

The atomic active center is the heart of SAzymes, which is similar to the cases of enzymatic and homogeneous catalysts. Compared with metal clusters and nanoparticles, the isolated single-atoms are all exposed on the surface as catalytic active centers, which play a critical role in the enzyme-like properties of SAzymes. The Fe-based single heme is the active site in natural

HRP. Zhu *et al*. reported that an Fe-based SAzyme with dense isolated Fe–N_4 sites displayed intrinsic POD-like performance to catalyze the oxidation of substrates such as TMB, o-phenylenediamine (OPD), and 2,2'-Azinobis-(3-ethylbenzthiazoline-6-sulphonate) (ABTS) (Jiao et al. 2020a). They also prepared other SAzymes containing M–N_4 sites, such as Co–N_4 and Zn–N_4 sites, and reported that their POD-like activity followed the order of Fe–N_4 > Co–N_4 > Zn–N_4 (**Figure 7a**). These similar coordination structures with different metal centers were provided as proof-of-concept models to clarify the metal-dependent POD-like catalytic mechanism. There were obvious differences in the bonding charge distributions among the different metal centers and coordinated N atoms (**Figure 7b**). In the POD-like catalytic process, the H_2O_2 molecule was first adsorbed on the metal centers of Fe–N_4, Co–N_4, and Zn–N_4 sites with the adsorption energy of −0.45, −0.36, and −0.40 eV, respectively, which indicated that Fe–N_4 possessed the highest POD-like catalytic activity. In addition to the POD-like activity, the OXD-like performance also showed a strong correlation with the metal centers in SAzymes (Wang et al. 2019d). Wang and coworkers found that the OXD-mimicking properties were highly dependent on the metal sites in the M–N_3 catalysts (M = Fe, Co, and Ni, **Figure 7c**). The SAzymes with the Fe–N_3 sites exhibited excellent OXD-like activity that was superior to those of Co–N_3 and Ni–N_3 configurations. The metal site-dependent enzymatic activities of the SAzymes were corroborated by theoretical studies. From the theoretical perspective, the thermodynamic reaction energies (E_r) for the homolytic cleavage of O_2 substrates increased in the order of Fe–N_3, Co–N_3, and Ni–N_3 catalysts (**Figure 7d**).

The enzyme-like property of SAzymes can also be regulated by the number of N coordinating the metal center. Unlike the typical SAzymes with M–N_3 and M–N_4 configurations, Dong and collaborators synthesized a series of SAzymes with carbon nanoframe-confined M–N_5 active centers (Huang et al. 2019a). The central metal atom was of great importance for the OXD-like behavior that showed the activity order of FeN_5 > MnN_5 > CoN_5 > NiN_5 > CuN_5 SAzymes.

Cheng's group paid particular attention to how different metal centers in SAzymes influenced various enzyme-like properties (Cao et al. 2022). By a universal metal–organic-precursor-based strategy, they successfully synthesized a series of SAzymes containing 20 different kinds of well-defined metal–N active sites as artificial metalloenzymes

(AMEs) and investigated their enzyme-mimicking activities and specificities. These AMEs could be developed as proof-of-concept models with similar geometries, including homologous morphology, diameters, surface areas, pore size, metal loading amounts, and metal–N_4 configuration (**Figure 7e**). Among all the AMEs they compared, Fe-AMEs exhibited the highest OXD-like catalytic activities with the fastest kinetics. Further study suggested that the POD-like catalytic activities were also strongly dependent on the active metal center. Cu-AMEs achieved the best POD-like performance while Co-AME possessed the lowest POD-like activity. Likewise, the halogen peroxidase (HPO)-mimetic catalytic behavior of these as-developed AMEs was assessed by the celestine blue (CB) method. HPO is a special class of POD enzymes that are used as efficient oxidants in antibacterial applications and it can oxidize halides to the corresponding hypohalites in the presence of H_2O_2. Ir-AMEs and Fe-AMEs showed outstanding HPO-like performance in oxidizing chloride to HOCl/OCl^-. These experimental results demonstrated that the OXD-, POD-, and HPO-like performances were closely related to the type of metal centers. In their theoretical investigation using DFT calculations, the Bader charge values in Fe–N_4 and Mn–N_4 active sites were much negative in comparison to the Co, Ni, and Cu AMEs (**Figure 7f**). More importantly, the degree of charge depletion in different metal sites of these AMEs was associated with the adsorption ability of enzyme substrates. The existence of delocalized charges around Co, Ni, and Cu centers would weaken the interaction with ROS intermediates and reduce the corresponding ROS-based catalytic reaction rate. In the process of H_2O_2-based ROS catalysis, Fe-AMEs with built-in Fe–N_4 active sites exhibited much stronger interaction with H_2O_2 than Mn-AMEs as evidenced by the Gibbs free energy diagram. There was also a much lower energy barrier for the generation of $^{\bullet}O_2^-$ intermediates on the surface of Fe-AMEs, suggesting a more thermodynamically favorable reaction path than the other metal-based AMEs. All these results suggested that the performance of SAzymes is closely related to the specific atomic metal centers. The tuning of the active single-atom centers is a direct and effective strategy for the rational designing of targeted SAzymes.

3.2. Heteroatom Tethering

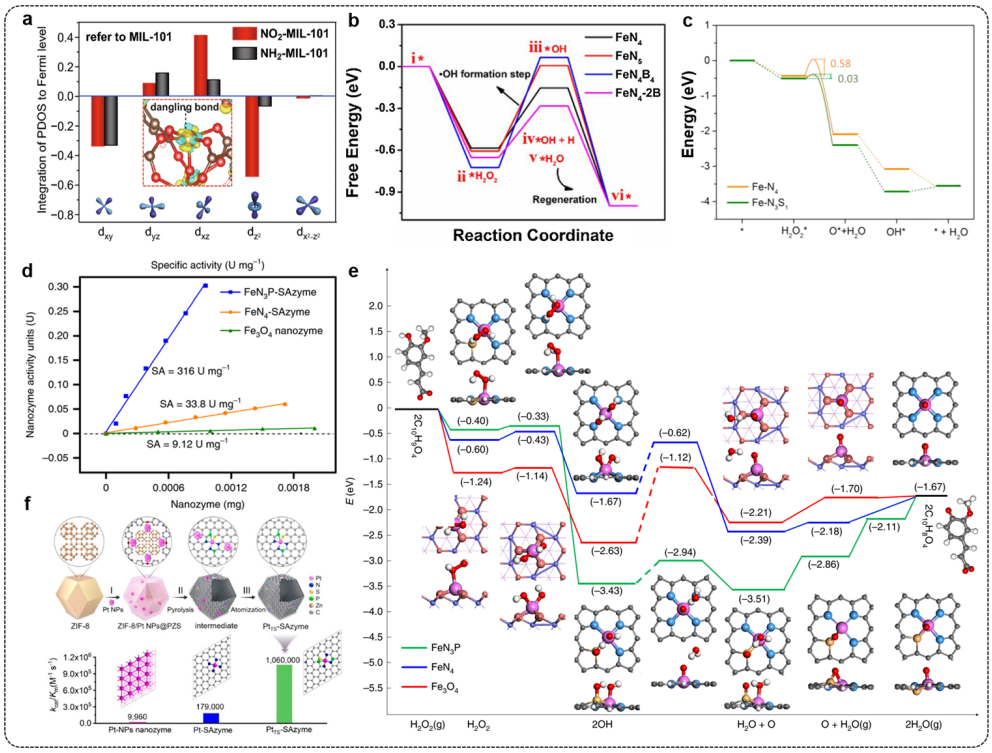

Figure 8. (a) Integration of PDOS and Fermi levels of each splitting 3d orbit of Fe single-atoms in NH_2-MIL-101 and NO_2-MIL-101 models (Xu et al. 2020). (b) Free energy diagram of optimized FeN_4, FeN_5, FeN_4B_4, and FeN_4-2B structures for the POD-like reaction in acidic media (Jiao et al. 2020b). (c) The corresponding free energy diagram of the POD-like process on the Fe–N_4 and FeN_3S_1 SAzyme models (Jiao et al. 2021). (d) Specific POD-like activities of engineered FeN_3P-centred active sites (FeN_3P-SAzyme), FeN_4-SAzyme, and Fe_3O_4 nanozyme. (e) Energy profile diagram of the POD-like reaction on the FeN_3P, FeN_4, and Fe_3O_4 models (Ji et al. 2021). (f) Schematic illustration of the fabrication of thermally stable Pt SAzyme (Pt_{TS}-SAzyme) and POD-like specific activities of the Pt-NPs nanozyme, Pt-SAzyme, and Pt_{TS}-SAzyme (Chen et al. 2021b). Reprinted with permission from references.

Heteroatoms in the second coordination sphere and beyond can be also considered as a potential factor. Heteroatom doping serves as a stabilization method for the single-metal atoms, and it could also induce the redistribution of the electron density around the isolated reactive centers (Li et al. 2020b). Moreover, the natural heme-based PODs employ a proximal histidine as an axial ligand *via* a strong hydrogen bond with the central Fe atom. It is also expected that the SAzymes with heteroatom doping or functional groups can display such specific enhancement in enzyme-like behavior. Zhu and collaborators fabricated MOF-based Fe POD-like SAzymes with different functional groups (Xu et al. 2020). The Fe single-atoms in the original MIL-101(Fe), similar to those in natural HRP, have five coordination. They introduced two kinds of functional groups, amino and nitro groups that possess the opposite charge characteristics, to the MIL-101(Fe). The NO_2-MIL-101 with an electron-withdrawing –NO_2

groups near the Fe active center exhibited better POD-like activity than the pristine MIL-101(Fe). On the contrary, the NH_2-MIL-101 nanozyme modified with an electron-donating –NH_2 group restrained the fundamental POD-like activity of MIL-101(Fe). The integration of projected electronic density of states (PDOS) and Fermi levels of each splitting 3d orbit of Fe atoms in NH_2-MIL-101 and NO_2-MIL-101 models confirmed these electronic effects (**Figure 8a**). The electron density of Fe–O bonds in the NO_2-MIL-101 decreased in the octahedral direction but increased along the non-bond direction. The integration of PDOS also indicated that the d_{z2} in the octahedral direction decreased while the d_{xz} on the non-bond orbit increased. By contrast, no significant differences in the integration of PDOS were observed from the NH_2-MIL-101 models. Such an electronic effect on the NO_2-MIL-101 could significantly activate the absorbed H_2O_2* species and reduce the energy barrier for HO* formation, which implies that heteroatom tethering could be a promising strategy for the engineering of high-performance nanozymes.

In addition to the aforementioned functional groups, heteroatoms can also be used for the modulation of the microenvironment around the active sites in SAzymes. Typical heteroatoms, such as N, O, B, P, and S that possess different atomic radii and electronegativity, are often engaged to alter the microenvironments of SAzymes. Taking some carbon-supported SAzymes as representative systems, Zhu's group successfully developed B-doped Fe–N–C (FeBNC) SAzymes using a one-pot pyrolysis process with boric acid (Jiao et al. 2020b). With B doping, the coordination number of single Fe atoms increased with a higher oxidation state in the FeBNC, which resulted in higher POD-mimicking activity and specificity than the pristine FeNC SAzyme. They further conducted DFT calculations to understand the role of B doping in determining the POD-like performance and thus uncover the reaction mechanism. Some types of FeBNC models, including four B atoms coordinated with N atoms around Fe atoms (FeN_4B_4) and two B atoms replaced with C atoms around FeN_4 centers (FeN_4-2B), were used for comparisons. The smaller electronegativity of B atoms than the neighboring C and N atoms resulted in a decrease in the positive charge toward the central Fe atoms, which could further lower the energy barrier in the POD-like process (**Figure 8b**). Such clear differentiation of electron densities was also proved by the Bader charge analysis. There was a close relationship between the Fe Bader charges in different models and the reaction energy barriers of the

generation of •OH species. All these results confirmed that B-doping would endow Fe–N–C SAzymes with exceptional POD-like activity and selectivity.

Sulfur atoms with a relatively large atomic radius could substantially affect the geometric and electronic structure of the central metal atom. In the recent work by Zhu and colleagues, isolated single-atom Fe sites anchored on the hierarchical S/N co-doped porous carbon (FeSNC) were fabricated *via* a template-assisted strategy (Jiao et al. 2021). The FeSNC SAzyme with unsymmetrically coordinated Fe–N_3S_1 sites delivered good POD-like activity compared with FeNC featuring only Fe–N_4 moieties. DFT calculations further revealed the source of the POD-like activity of FeSNC SAzyme. The differences in the charge density (q_{Fe}) of the Fe–N_3S_1 models confirmed the relatively high oxidation state of Fe atoms. The electronic interaction between the adsorbed H_2O_2 intermediates and Fe active sites on the Fe–N_3S_1 model was much stronger than that of Fe–N_4 structures. The incorporation of S atom in the FeSNC SACs could activate the O=O bonding and lengthen the O–O distance in the adsorbed H_2O_2 species, which resulted in the accelerating of the overall POD-like catalytic reaction (**Figure 8c**).

In an attempt to boost the kinetics of SAzymes to match that of natural enzymes, Li *et al.* constructed a POD SAzyme by modulating FeN_3P-centred active sites (FeN_3P-SAzyme) (Ji et al. 2021). FeN_3P-SAzyme displayed well-defined electronic and geometric structures, which made it a suitable candidate for SAzymes with high catalytic activity and kinetics. The as-constructed FeN_3P-SAzyme possessed higher measured specific activity (316 U mg^{-1}) than those FeN_4-SAzymes without P coordination (33.8 U mg^{-1}) and the most widely used Fe_3O_4 nanozyme (**Figure 8d**). These findings demonstrated that FeN_3P-SAzyme possessed the fundamental characteristics of natural enzymes, including fast kinetics, substrate specificity, and high efficiency. The effect of P and N doping on Fe SAzymes was further explored by DFT calculations. The local electronic structure of the Fe atoms in FeN_3P-SAzymes carried less positive charge due to the electron-donating nature of the neighboring P atom. The comparison of the oxidation process of POD substrates on three catalyst models of FeN_3P-SAzyme, FeN_4-SAzyme, and Fe_3O_4(111) indicated that the H_2O_2 dissociation into surface O species was thermodynamically more favorable on the FeN_3P-SAzyme models (**Figure 8e**). The strong affinity for the TMB substrate with the generated OH and O species on the P site facilitated the POD-like catalytic efficiency as well. The synergistic effects of the Fe and P atoms in the

FeN_3P-SAzyme could be a promising strategy for regulating the inherent properties of SAzymes.

In another study by the same group, a thermally stable Pt SAzyme (Pt_{TS}-SAzyme) with a unique Pt_1-N_3PS active moiety was developed (**Figure 8f**) (Chen et al. 2021b). By the atomization of Pt NPs into single atoms, the active site was fully exposed and superior POD-like catalytic activity was realized. Pt_{TS}-SAzyme also displayed significantly enhanced catalytic rate constant (k_{cat}) and catalytic efficiency (k_{cat}/K_m), which far exceeded those of the Pt nanoparticle nanozyme and Pt SAzyme (Pt-SAzyme). The theoretical analysis illustrated the role of heteroatom doping of P and S atoms. First, in the atomization process from the Pt_{10} cluster to the Pt single atom, the introduction of P and S elements promoted the single Pt atom formation with a low energy barrier. Furthermore, the synergistic effects of Pt, N, P, and S atoms in Pt_1-N_3PS-SAzyme significantly modified the electronic structure by pushing the electron density from P atoms to N and S atoms, which could effectively promote the whole POD-like catalytic process. The Pt_{TS}-SAzyme with P, S co-doped structures was experimentally proven to provide suitable thermodynamic adsorptions for the POD substrates (H_2O_2 and TMB). Benefiting from heteroatom tethering, other kinds of SAzymes were also designed with excellent and specific enzyme-like activity. For instance, B atoms were successfully introduced into Zn-N-C SAzymes (ZnBNC) that showed super POD-like activity (Feng et al. 2022). The OXD-like performance of Fe SAzymes could also be promoted by the doping of S atoms (Li et al. 2022a).

3.3. Regulation of Coordination Number of Single-Atom Sites

The adjustment of the coordination numbers of the metal center also offers a useful way of tuning the electronic structure around the active sites in SAzymes. Cui's group investigated the effect of the coordination numbers of SAzymes on the OXD-like activity (Wang et al. 2019d). Firstly, the adsorption energies of O_2 substrates on Fe SAzymes models of various coordination numbers, including Fe–C_3, Fe–N_3/C, Fe–N_4/C, and Fe–N_5/C, were investigated by DFT calculations (**Figure 9a**). The OXD-like activity of the Fe SAzymes was found to be sensitive to the coordination number, and the Fe–N_3/C structure demonstrated the highest chemical reactivity towards the O_2 substrate (**Figure 9b**). The coordination number-dependent OXD-

like activity was experimentally verified by constructing representative Fe–N_3/C and Fe–N_4/C SAzymes (**Figure 9c**).

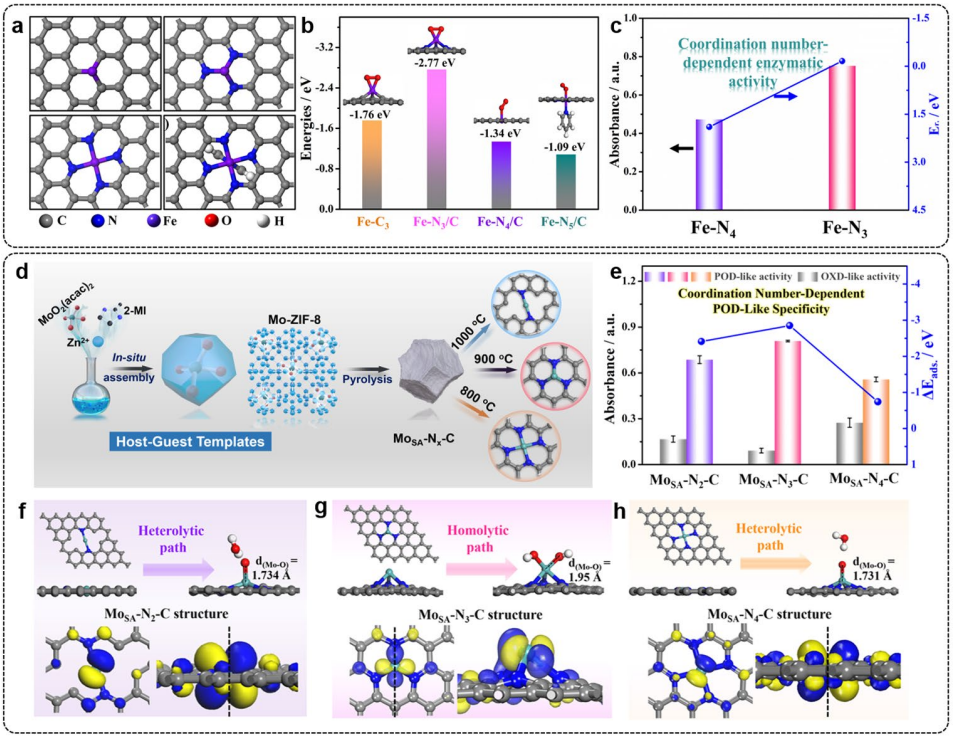

Figure 9. (a) Schematic OXD-like models of the Fe-centered SAzymes with various coordination numbers (Fe–C_3, Fe–N_3/C, Fe–N_4/C, and Fe–N_5/C). (b) Adsorption energy of O_2 substrates on Fe–C_3, Fe–N_3/C, Fe–N_4/C, and Fe–N_5/C structures. (c) Coordination number dependency of OXD-like activity and theoretical thermodynamic energy (Wang et al. 2019d). (d) Schematic depiction of the synthesis process for the Mo_{SA}-N_x-C with various coordination numbers. (e) Coordination number dependency of POD-like specificity and H_2O_2 and O_2 adsorption energies among Mo_{SA}-N_2-C, Mo_{SA}-N_3-C, and Mo_{SA}-N_4-C catalysts. Possible decomposition process of H_2O_2 by hemolytic and heterolytic path, and the corresponding highest occupied molecular orbital (HOMO) structures on (f) Mo_{SA}-N_2-C, (g) Mo_{SA}-N_3-C, and (h) Mo_{SA}-N_4-C catalysts (Wang et al. 2021d). Reprinted with permission from references.

Cui's group investigated the possibility of enhancing the specificity in POD-like catalysis by tuning the coordination number of active sites in SAzymes (Wang et al. 2021d). They fabricated a series of single atomic Mo catalysts (Mo_{SA}-N_x-C) by pyrolyzing host–guest templates (**Figure 9d**). These well-defined Mo_{SA}-N_x-C catalysts with different Mo–N_x coordination numbers (x = 2, 3, and 4) were successfully constructed by controlling the pyrolysis temperatures, and they were named Mo_{SA}-N_4-C, Mo_{SA}-N_3-C, and Mo_{SA}-N_2-C, respectively. By monitoring the absorbance changes at 652 nm, they studied the specific POD-like behaviors of these Mo_{SA}-N_x-C catalysts and successfully demonstrated that the POD-like and OXD-like properties were affected by the Mo–N coordination number (**Figure 9e**). The

Mo_{SA}-N_3-C SAzyme displayed supreme POD-like performance but the lowest OXD-like activity. Subsequently, the origin of this specific POD-like behavior was examined by DFT calculations. The dissociation products for H_2O_2 molecules were highly dependent on the coordination of the Mo atoms. There was a heterolytic path for the dissociation of adsorbed H_2O_2 into (O* + H_2O) intermediates on both Mo_{SA}-N_2-C and Mo_{SA}-N_4-C SAzymes (**Figures 9f** and **9h**). In contrast, two OH* species were generated by a homolytic path on the Mo–N_3 moiety (**Figure 9g**). Such a different dissociation way was attributed to the atomic structure and orientation of frontier molecular orbitals of these Mo_{SA}-N_x-C catalysts. Based on the maximum overlapping principle in the molecular orbital theory, they showed that there was better symmetry matching between the HOMO of Mo atoms and the LUMO of H_2O_2 species on Mo–N_3 structures by horizontal adsorptions, whereas the H_2O_2 adsorption on Mo–N_2 and Mo–N_4 moieties involved a vertical configuration (**Figures 9f – 9h**). This work demonstrated the importance of active site configuration in SAzymes in promoting the targeted enzyme-like property.

3.4. Synergetic Interaction between Neighboring Species

For most enzyme-like reactions, there are multiple reaction intermediates and complicated proton-coupled electron transfer processes. It is thus difficult for the SAzymes possessing only one type of metal center to break the scaling relationship in many enzyme-like reactions. There has been much effort to adopt multiple structural and electronic promotions *via* synergetic active site engineering, support strain engineering, and constructing dual metal sites to promote SAzyme performance. Zhu and co-workers engineered single-atom Fe centers coupled with carbon-encapsulated Fe_3C crystals (Fe_3C@C/Fe-N-C) by a spatial confinement strategy (**Figure 10a**) (Xi et al. 2021). Compared with the conventional Fe SAzymes, the introduction of the Fe_3C@C nanocrystals in the Fe_3C@C/Fe-N-C nanozyme resulted in synergistically enhanced POD-like activity. DFT calculations provided further insight into the role of Fe_3C nanocrystals in the POD-like reaction. The electron transfer from Fe_3C@C to single atomic Fe sites resulted in a more energy-favorable POD-like reaction on the Fe_3C@C/Fe-N-C model (**Figure 10b**). Considering that the multi-enzyme-mimicking SAzymes relied on the cofactor and microenvironment, the behavior of multi-enzymatic SAzymes could also be evaluated by

this strategy. So a nanozyme-based artificial peroxisome (*pero*-nanozysome) was rationally designed by integrating Fe–N_4 and Fe clusters as a prosthetic group and reversible cofactors, respectively (**Figure 10c**) (Xi et al. 2021). Similar to natural peroxisome, this *pero*-nanozysome showed multiple peroxisomal-like activities, including POD-, OXD-, CAT-, SOD-, and urate oxidase (UOD)-like activities, which were pH-dependent.

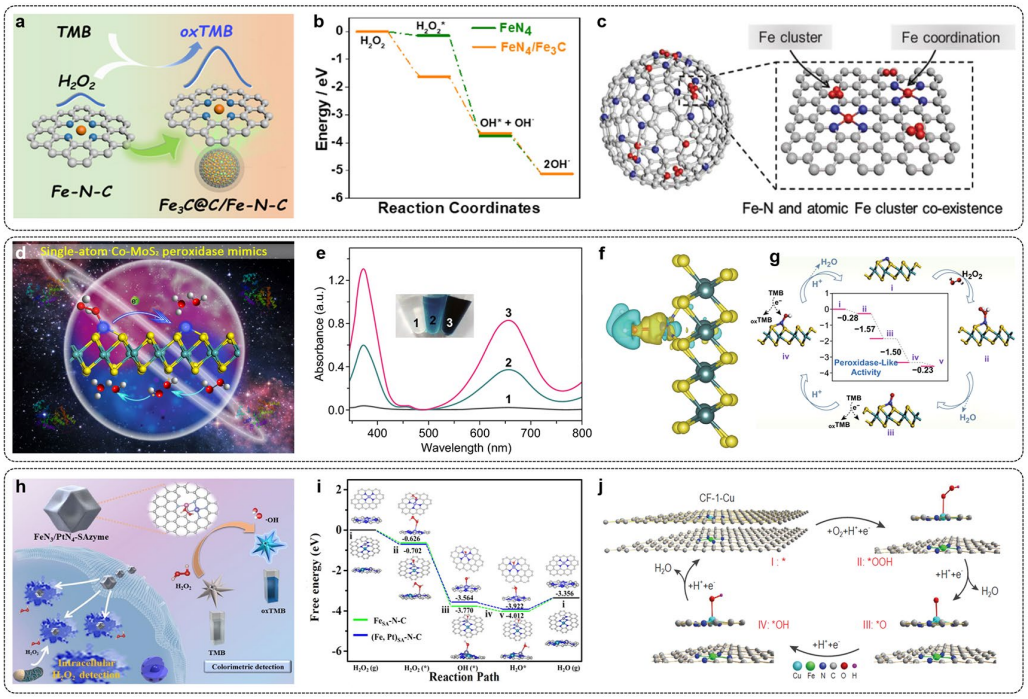

Figure 10. (a) Schematic illustration of single atomic Fe sites coupled with carbon-encapsulated Fe_3C nanoparticles (Fe_3C@C/Fe-N-C) and Fe-N-C SAzymes with POD-like activity. (b) Predicted free energy profiles of the POD-like reaction on Fe_3C@C/Fe-N-C and Fe-N-C models (Xi et al. 2021). Schematic illustrations of (c) artificial peroxisome by constructing Fe–N_4 as a prosthetic group and Fe clusters as reversible cofactors (*pero*-nanozysome) with multiple enzyme-like activities (Xi et al. 2021) and (d) heterogeneous single-atom Co-MoS_2 (SA Co-MoS_2) POD-like SAzymes. (e) UV–vis spectra in various POD-like systems: (1) TMB + H_2O_2, (2) TMB + H_2O_2 + MoS_2, and (3) TMB + H_2O_2 + SA Co-MoS_2. (f) Charge density difference for the adsorbed H_2O_2 substrates on the SA Co-MoS_2. (g) Free energy diagram and the corresponding optimized structures of H_2O_2 dissociation on SA Co-MoS_2 (Wang et al. 2019c). (h) Schematic diagram of atomically dispersed Fe, Pt binuclear catalysts with unique Fe–N_3/Pt–N_4 moieties ((Fe, Pt)$_{SA}$-N-C) as excellent POD-like SAzymes. (i) Free energy profiles for the (Fe, Pt)$_{SA}$-N-C and Fe_{SA}-N-C in POD-like reaction (Wang et al. 2022a). (j) Proposed free energy diagram for the OXD-like reaction on the single-atom Fe nanozyme (F-HNCS) and hetero-binuclear Cu–Fe centres on hollow N-doped carbon spheres (CF-HNCS) (Lu et al. 2022). Reprinted with permission from references.

Similar to the typical electronic metal–support interaction in many metal-based nanomaterials, single metal atoms that are anchored on support also display phase and structural modifications of the support. In the work conducted by Cui *et al.*, single-atom Co sites anchoring on the distorted 1T phase MoS_2 (SA Co-MoS_2) were fabricated as a

proof-of-concept nanozyme model (**Figure 10d**) (Wang et al. 2019c). The well-defined structure of SA Co-MoS_2 achieved significantly enhanced POD-like catalytic performance (**Figure 10e**). Moreover, unlike the typical Fenton-like mechanism of pristine MoS_2, the enhanced POD-like catalytic activity of SA Co-MoS_2 did not rely on the Fenton-like reaction. The adsorption energies (E_{ads}) of H_2O_2 and TMB substrates were evaluated by DFT analysis to reveal that SA Co-MoS_2 exhibited a higher affinity for H_2O_2, and MoS_2 was more likely to adsorb TMB (**Figure 10f**). As a result, there were different POD-like catalytic pathways in the SA Co-MoS_2, where the single-atom Co relied on the electron transfer mechanism and MoS_2 supports preferred the Fenton-like reactions. Overall, the synergetic effect by the strain engineering of a single Co atom on the supports caused the negative thermodynamic energy for the POD-like reaction (**Figure 10g**).

The structural simplicity of SAzymes makes it difficult to break the linear scaling relationship limit of different intermediates. As an expansion of SACs, dual-atom catalysts (DACs) not only inherited the advantages of SACs but also expanded the active sites and metal loadings (Zhang et al. 2021b; Wang et al. 2022d). Zheng and co-workers developed atomically dispersed Fe, Pt binuclear catalysts ((Fe, Pt)$_{SA}$-N-C) featuring the unique Fe–N_3/Pt–N_4 moieties *via* a secondary-doping strategy (Wang et al. 2022a). The obtained (Fe, Pt)$_{SA}$-N-C nanozyme exhibited superior POD-like activity and Fenton-like catalytic performance owing to the synergistic effect of two metal atoms (**Figure 10h**). Further insight into the mechanism of Fenton-like reactions and the synergistic effect of Fe–Pt dual-metal configuration was gained by DFT calculations (**Figure 10i**). The reduction of H_2O_2 substrates on the surface of (Fe, Pt)$_{SA}$-N-C proceeded with a lower energy barrier than that in the Fe$_{SA}$-N-C with Fe–N_4 moieties *via* a proton-mediated H_2O_2 homolytic pathway. Coincidentally, in a recent work done by Shi and co-workers, hetero-binuclear Cu–Fe centers constrained on hollow N-doped carbon spheres (CF-HNCS), which was inspired by natural heme-copper oxidase, were reported (Lu et al. 2022). The synergistic catalytic effect of the biomimetic binuclear Cu–Fe centers in the CF-HNCS facilitated enhanced OXD-like activity. Based on the free energy profiles for the OXD-like reaction, the CF-HNCS model with Cu–Fe dual-atom sites displayed the optimal adsorption strength of oxygen intermediates (**Figure 10j**).

4. Biosensing Applications of SAzymes

Benefiting from the distinct active sites and adjustable configurations of SACs, SAzymes demonstrated remarkable enzyme-like catalytic behaviors with satisfactory activity, specificity, and stability. Especially in the analytical field, SAzymes could provide amplified signals with high sensitivity, good selectivity, fast response, and long-term stability. In this section, we would focus on the recent progress made in diverse biosensing applications of SAzymes, including colorimetric, electrochemical, photoelectrochemical, fluorescence, chemiluminescence, electrochemiluminescence biosensing, and dual-model biosensors.

4.1. Colorimetric Biosensing

Colorimetric biosensing offers the advantages of simplicity, low cost, and sensitive detection and holds great promise in the detecting of target substrates by the naked eye or simple portable optical devices. SAzymes have been widely used in the rational fabrication of various colorimetric biosensing platforms. Especially, the Fe–N–C SAzymes with Fe–N_x active sites were proved as suitable candidates to mimic natural HRP with desirable POD-like activity. As a proof-of-concept application, Lee and colleagues developed an Fe SAzyme (Fe-N-rGO) featuring high and selective POD-like activity (Kim et al. 2019) and used it as a sensitive colorimetric probe for detecting acetylcholine in human blood samples. In the bioassay application, trace amounts of H_2O_2 released from human cancerous cells were also successfully quantified with high sensitivity. Likewise, Zhu and co-workers successfully established a biological platform based on the Fe–N–C POD-like SAzymes (Jiao et al. 2019; Jiao et al. 2020a). This colorimetric biosensing assay achieved good linear correlation and acceptable repeatability in H_2O_2 detection. Furthermore, the biosensing method was successfully applied for *in situ* detection of H_2O_2 released from the Hela cells (**Figure 11a**). In addition, a series of paper-based bioassays based on the Fe POD-like SAzymes were successfully constructed for the ultrasensitive colorimetric analysis of H_2O_2, glucose, and ascorbic acid (Cheng et al. 2019). A heteronuclear FeN_3/PtN_4-SAzyme facilitated the colorimetric biosensing of dopamine and was used for *in situ* detection of intracellular H_2O_2 (Wang et al. 2022b).

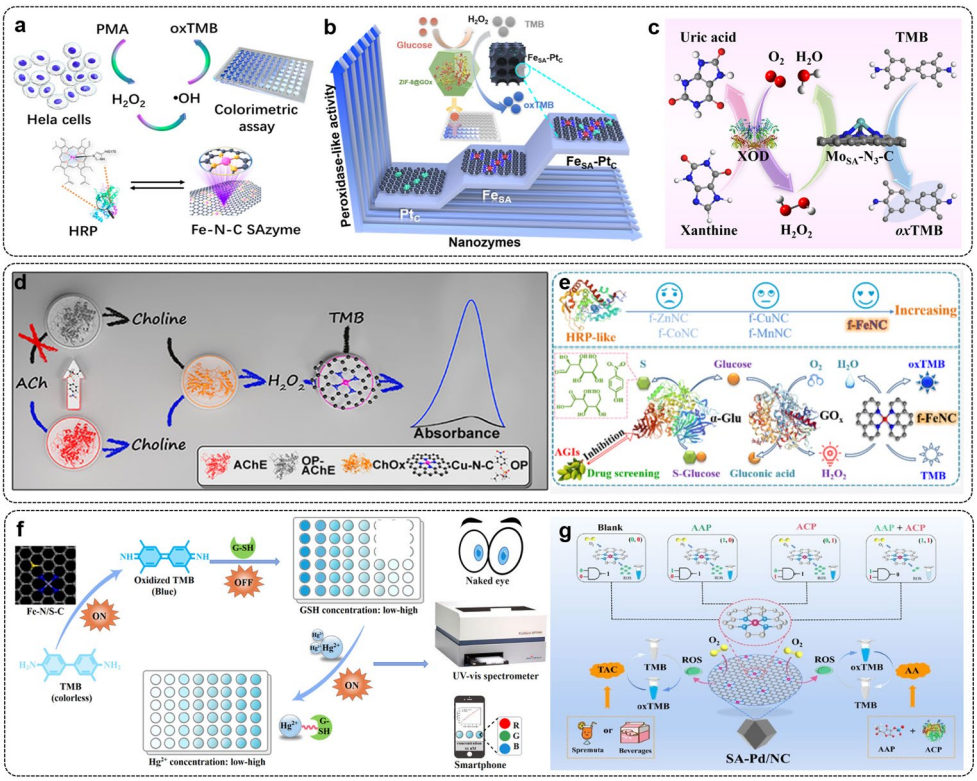

Figure 11. Schematic illustrations of (a) Fe–N–C SAzymes for the colorimetric biosensing detection of intracellular H_2O_2 molecules (Jiao et al. 2019) and (b) Fe_{SA}-Pt_C nanozyme-based signal amplification strategy for the detection of PSA by Fe_{SA}-Pt_C-ZIF-8/GO_x ELISA (Chen et al. 2021a). Schematic illustrations of (c) colorimetric detection of xanthine by the POD-like Mo_{SA}–N_3–C nanozyme (Wang et al. 2021d), (d) colorimetric sensing of AChE activity and OPs (Wu et al. 2020b), (e) versatile SAzyme and natural enzyme cascade-based colorimetric bioassays (Zhang et al. 2022a), (f) Fe–N/S–C-based colorimetric biosensing for the detection of GSH and Hg^{2+} (Li et al. 2022a), and (g) Pd SAzyme to evaluate total antioxidant capacity of fruit and serum acid phosphatase activity, and construct the NAND logic gate (Li et al. 2022c). Reprinted with permission from references.

Numerous SAzyme-involved cascade reaction systems have been established to mimic biological cascade catalytic reactions. The glucose oxidase-peroxidase (GO_x-POD) cascade catalytic system is one of the most common platforms in glucose biosensing applications. For instance, a simple colorimetric biosensor using an Fe–N–C POD-like SAzyme and GO_x cascade platform was fabricated to achieve reliable visualization of glucose targets (Chen et al. 2020). Zhu and co-workers reported a cascade signal amplification strategy based on the natural GO_x and Fe_{SA}–Pt_C POD-like SAzyme cascade catalyst (**Figure 11b**) (Chen et al. 2021a). This proposed cascade catalytic nanoreactor was employed with the traditional enzyme-linked immunosorbent assay (ELISA) to detect prostate-specific antigens (PSA). Interestingly, wide linear ranges (from 8 to 1,000 pg mL^{-1}) and low limits of detection (LOD, 1.8 pg mL^{-1}) were achieved by this colorimetric immunoassay method. Other kinds of biomimetic cascade

nanoreactors have also been developed for diverse cascade reaction systems (Cai et al. 2021; Zhang et al. 2021c). Cui's group utilized the Mo_{SA}–N_3–C POD-like SAzyme with comparable activity and substrate specificity to construct a POD-xanthine oxidase cascade reaction system (**Figure 11c**) (Wang et al. 2021d). The proposed colorimetric assay could successfully recognize xanthine in human serum samples.

Wu and coworkers demonstrated another biomimetic cascade nanoreactor using a three-enzyme system (AChE-ChO_x-POD), namely acetylcholinesterase (AChE), choline oxidase (ChO_x), and Cu–N–C POD-like SAzymes (**Figure 11d**) (Wu et al. 2020b). The hydrolysis of acetylcholine was catalyzed by AChE to form choline substrates, which were further oxidized by ChO_x to generate H_2O_2 molecules. Subsequently, by taking advantage of the remarkable POD-like activity of Cu–N–C SAzymes, the produced H_2O_2 was decomposed into ROS by POD-like activity. As a concept application, this three-enzyme-based cascade reaction system was used for the colorimetric detection of acetylcholine and organophosphorus pesticides (OPs) with high sensitivity and selectivity. Wu and coworkers also reported two other kinds of POD-like SAzymes, B-doped Fe–N–C SAzyme and Fe–N_3S_1 SAzyme. Two efficient cascade catalytic bio-platforms were successfully developed by these two POD-like SAzymes for colorimetric detection of acetylcholine and organophosphorus pesticides. Guided by this concept, a Ce–N–C POD-like SAzyme was integrated with a 3D-printed platform to fabricate bioactive papers (Song et al. 2022). By combining Ce–N–C SAzymes with AChE-based cascaded catalytic reactions, portable on-site testing was achieved toward various pesticide residues in fruits and vegetables. More recently, a versatile three-enzyme cascade-based catalytic nanoreactor was established by combining the Fe–N–C POD-like SAzyme with GO_x and α-glucosidase (α-Glu, **Figure 11e**) (Zhang et al. 2022a). This α-Glu/GO_x/Fe–N–C cascade reaction-based colorimetric assay was used for evaluating α-Glu activity and further employed to screen α-Glu inhibitors as suitable anti-diabetic and antiviral drugs.

The biomimetic OXD-like SAzymes were also developed for excellent colorimetric biosensing. For example, Co–N–C SAzymes with high OXD-like activity could directly oxidize TMB substrate to $_{ox}$TMB without the addition of H_2O_2 (Sun et al. 2022). Some typical biothiols with the feature of Lewis bases could bind to the single atom center in SAzymes. A colorimetric biosensing platform for the selective detection of GSH and cysteine (Cys) was

successfully developed based on the inhibition of the OXD-like activity of Co–N–C SAzymes. Moreover, a feasible colorimetric platform for GSH detection was also proposed on the basis of the superior OXD-like Fe SAzyme (Wang et al. 2019d). A novel switching on–off–on colorimetric sensor using Fe–N/S–C SAzymes was well established for the ultra-sensitive detection of GSH (off) and Hg^{2+} (on) (Li et al. 2022a). It was feasible to acquire signals for the quantitative analysis using different modes such as the naked eye, UV–vis spectrometer, and smartphone (**Figure 11f**). Later, the cascade catalytic system was also constructed by a combination of a natural enzyme and biomimetic OXD-like SAzymes (Cai et al. 2021). A total antioxidant capacity colorimetric assay based on the Pd SAzyme provided satisfactory sensitivity and selectivity for evaluating the antioxidant capacity (**Figure 11g**) (Xu et al. 2022). The coupling of acid phosphatase with a biomimetic Pd SAzyme was also demonstrated for the determination of acid phosphatase.

4.2. (Photo)Electrochemical Biosensing

In addition to colorimetric biosensing, electrochemical biosensors also attracted immense attention as a suitable platform to integrate SAzymes due to their advantages of easy operation, cost-effectiveness, favorable sensitivity, and *in situ* real-time monitoring. Besides, the coupling of SAzymes with electrochemical biosensors could amplify the electrochemical signal. Zhu and colleagues synthesized an atomically dispersed Ir–N–C SAC through a template-assisted method (Luo et al. 2022), which showed excellent ORR activity. This Ir SAzyme was integrated with AChE to serve as an electrochemical sensing platform for the detection of organophosphorus pesticides (**Figure 12a**). The catalytic current density displayed a good correlation with the logarithm of organophosphorus pesticide concentrations with high sensitivity and selectivity (**Figure 12b**). A POD-like Fe_3C@C/Fe–N–C SAzyme was also developed by the same group as a H_2O_2 electrochemical sensor with superior sensitivity (LOD = 0.26 μM) and selectivity (**Figure 12c**) (Xi et al. 2021). Remarkably, the Fe_3C@C/Fe–N–C-based H_2O_2 electrochemical biosensor could be used for monitoring trace amounts of H_2O_2 released from living cells. Another electrochemical biosensing platform was fabricated using a single-atom Ru biomimetic SAzyme (**Figure 12d**) (Xie et al. 2021). Taking advantage of the high sensitivity, selectivity, and stability in detecting the oxidation of dopamine (DA) and uric

acid (UA), this Ru SAzyme-based biosensor could successfully recognize DA and UA in real biological serum samples. Similar simultaneous UA detection was also achieved by a Co SAC-based electrochemical biomimetic sensor (**Figure 12e**) (Wu et al. 2020b). The wide linear detection ranges and low detection limits of this Co SAzyme-based biosensor could meet the requirements of practical diagnosis.

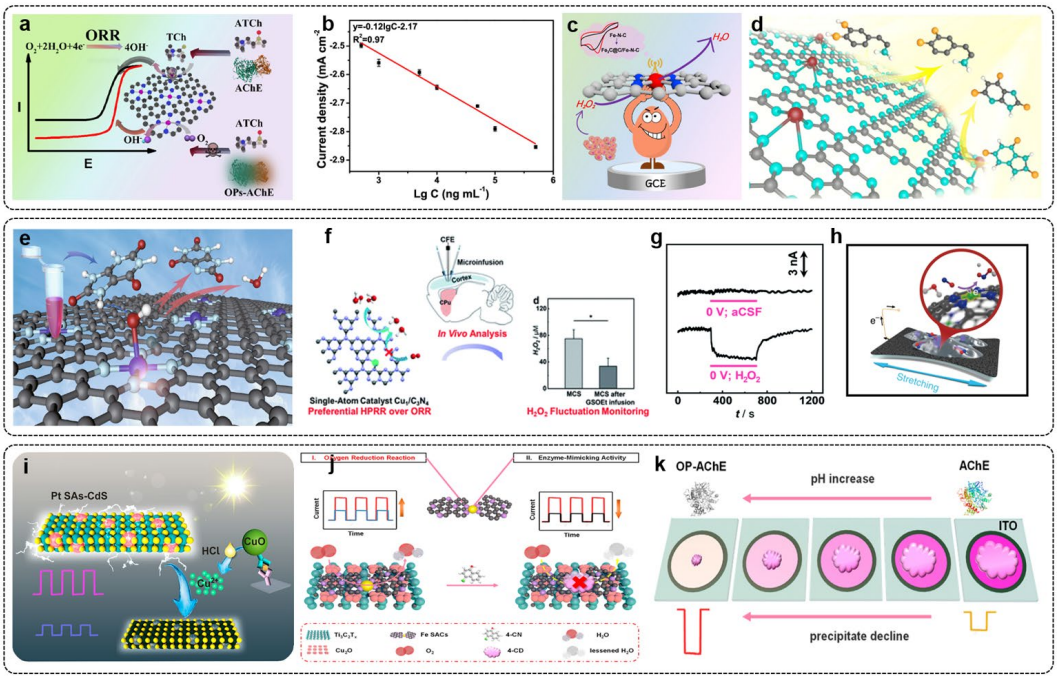

Figure 12. (a) Schematic diagram for the electrochemical detection of OPs based on AChE and Ir SAzymes. (b) Linear relation between the logarithm of OP concentration and current values based on AChE-Ir SAzyme-based biosensor (Luo et al. 2022). Schematic diagrams of (c) electrochemical H_2O_2 sensing platform based on the Fe_3C@C/Fe-N-C (Xi et al. 2021), (d) electrochemical DA and UA sensing platform based on the Ru SAC biomimetic enzyme (Xie et al. 2021), (e) Co SAC-based electrochemical biosensor for the detection of UA (Wu et al. 2020b), and (f) electrochemical sensing platform based on the Cu SAC for *in vivo* monitoring of H_2O_2. (g) Typical amperometric responses on the electrochemical microsensor implanted into the cortex of anesthetized guinea pigs (Gao et al. 2021). Schematic illustrations of (h) Ni SACs/N-C-based stretchable sensor for the real-time monitoring of the nitric oxide (NO) released from cells (Zhou et al. 2020), (i) Pt SAC-CdS-based ultra-sensitive PEC biosensing platform (Qin et al. 2021), and (j) Fe SACs/Cu_2O/$Ti_3C_2T_x$-based PEC biosensing platform. (k) Biosensing mechanism of Fe SACs/Cu_2O/$Ti_3C_2T_x$-based PEC biosensor (Qin et al. 2022). Reprinted with permission from references.

These SAzyme-based electrochemical biosensors provided a new strategy for on-line and *in vivo* analysis of living organisms. Very recently, Mao's group developed a Cu–N_2 SAzyme-based biosensing platform for selective electrochemical H_2O_2 reduction reaction (HPRR) rather than ORR (**Figure 12f**) (Gao et al. 2021). By virtue of the preference to H_2O_2 over O_2 molecules, a Cu–SAC-based microsensor achieved a good H_2O_2 response without O_2 interferences.

Typical amperometric responses could be seen from this real-time monitoring biosensor with the local infusion of H_2O_2 into the rat cortex (**Figure 12g**). This result confirmed the promising *in vivo* application of SAzymes in the real-time quantitative investigation. Mao's group also discovered that the Co SAC-based electrochemical biosensor could display a good response at low applied potentials (Hou et al. 2019). An online electrochemical system with this OXD-Co-SAC-based glucose biosensor produced good responses for the monitoring of microdialysate glucose in rat brains. They further fabricated a Ni SACs-based flexible and stretchable sensor for another signaling molecule of NO gas in a live cellular environment (**Figure 12h**) (Zhou et al. 2020). This stretchable electrochemical sensor was successfully applied for the real-time monitoring of NO released from human umbilical vein endothelial cells.

The photoelectrochemical (PEC) biosensing combines the advantages of both electrochemical and optical techniques, and it has been widely recognized as a useful sensing technique. Benefiting from the excellent sensing modalities of SAzymes, the photoinduced current signal can be well amplified by single-atom-based photoactive nanomaterials. As a proof-of-concept, Pt single atoms supported by CdS nanorods (Pt SAs-CdS) were prepared to fabricate an ultra-sensitive PEC biosensor (**Figure 12i**) (Qin et al. 2021). By the introduction of positively charged Pt SAC, the PEC signal of this enzyme-free Pt SAzyme–CdS immunoassay was significantly improved by the fast transfer of photogenerated electrons and the high-efficiency separation of electron-hole pairs. As a result, this PEC biosensing platform, which held promising applicability in practical applications, was employed for the highly sensitive detection of PSA with a low LOD of 0.92 pg mL^{-1}. In addition, this group further expanded the single-atom-involved PEC biosensing platform by making use of the comparable POD-like activity and ORR performance of well-defined Fe SACs (Qin et al. 2022). A Fe SACs/Cu_2O/$Ti_3C_2T_x$-based PEC biosensing platform was rationally designed by taking $Ti_3C_2T_x$ MXene with high mobility of holes as suitable support and Cu_2O nanoparticles as a typical *p*-type semiconductor (**Figure 12j**). The boosted PEC biosensing mechanism for the detection of AChE activity and organophosphorus pesticides was as follows: 4-chloro-1-naphthol was oxidized into insoluble precipitates by the POD-like Fe SAzymes; The photocurrent response of the PEC biosensor could be depressed by these precipitates; Coupled with the Fe SAzyme-involved cascade reaction systems, the AChE activity and organophosphorus pesticides could

be quantitatively analyzed by the synergistic amplification with high sensitivity and excellent selectivity (**Figure 12k**). Furthermore, this PEC biosensing also displayed pH-regulated POD-like activity.

4.3. (Electro)Chemiluminescence Biosensing and Others

Chemiluminescence (CL) is another powerful analytical technique based on the light emission process of an excited electronic molecular state returning to the ground state. SAzymes with outstanding enzyme-like performance can be well designed for the catalytic production of ROS. The combination of typical luminol-based CL systems and emerging SAzymes shed new light on a broad spectrum of desirable CL biosensing applications. In 2017, graphene oxide nanoparticles modified with single metal Cu(II) ions (Cu^{2+}-GO NPs) were reported as a heterogeneous catalyst mimicking HRP and NADH peroxidase (Wang et al. 2017b). These Cu^{2+}-GO NPs with POD-like properties enabled the decomposition of H_2O_2 and then the oxidation of dopamine to aminochrome with the formation of CL signals. This Cu^{2+}-GO NPs/luminol/H_2O_2 CL system was implemented for the biosensing analysis of H_2O_2 and the activity evaluation of H_2O_2-generating oxidases. A similar single metal atom-based CL system was prepared by Cui's group with the Co^{2+}-GO-catalyzed lumino-H_2O_2 reaction (Wang et al. 2017a). In another research, an effective CL system was established by employing Co SAC as a singlet oxygen ($^1O_2$) generated accelerator (**Figure 13a**) (Ouyang et al. 2020). The corresponding CL immunoassay (CLIA) method could display satisfactory selectivity of the cardiac troponin I analysis. Fu and coworkers also utilized Co-SAC as the CL probe in the CLIA for sensitive detection of aflatoxin B1. High sensitivity (LOD = 0.44 pg mL^{-1}) and good linear correlation (10 – 1,000 pg mL^{-1}) for aflatoxin B1 analytes confirmed the application potential of this CL biosensing platform.

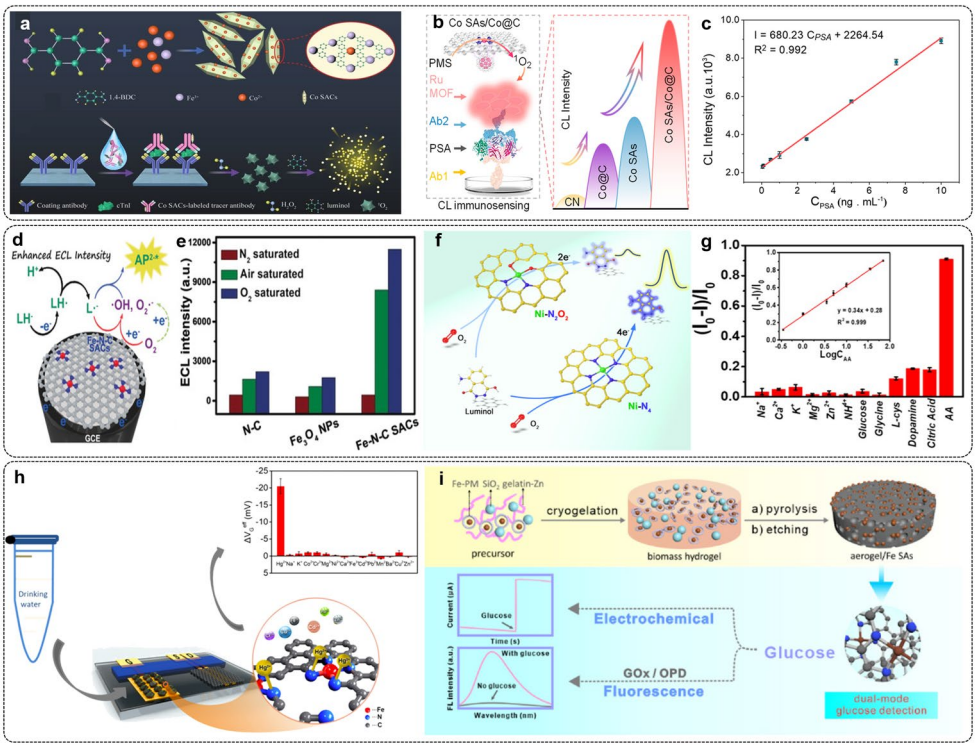

Figure 13. Schematic illustrations of (a) preparation of Co SAC and the CLIA method for cardiac troponin I (cTnI) analysis (Ouyang et al. 2020) and (b) Ru MOF/Co SAs/Co@C/PMS system with the synergistic effect for the enhanced CL performances. (c) Linear relationship between the concentration of PSA and CL intensity (Wu et al. 2022). (d) Schematic of Fe-N-C SAC-luminol-O_2 ECL sensing platform. (e) ECL intensity of N-C, Fe_3O_4 NPs, and Fe–N–C SAC in N_2, air, and O_2-saturated solution (Gu et al. 2020). (f) Schematic representation of the different ECL mechanisms based on Ni SAC. (g) Selectivity of the proposed Ni SAC-luminol-ECL biosensing assay. Inset is the linear relationship between the concentration of AA and ECL intensity (Xie et al. 2021). Schematic illustration of (h) SGGT functionalized by Fe SAzymes to real-time monitoring of Hg^{2+} (Yao et al. 2020) and (i) dual functional detection platform based on a Fe POD-like SAzyme (Gao et al. 2021). Reprinted with permission from references.

Very recently, a novel tris-(bipyridine)-Ru(II)-based ternary CL system ($[Ru(bpy)_3]^{2+}$) was fabricated by Wu and coworkers using a Co SAzyme (Wu et al. 2022). They successfully utilized the synergistic effect of the Co SAC and carbon-encapsulated Co nanoparticles (Co@C) to realize selective peroxymonosulfate activation to generate sufficient $^1O_2$ species. Thus, the response for the $[Ru(bpy)_3]^{2+}$-based CL system could be significantly enhanced. This proposed ternary CL system was further used for the quantitative determination of peroxymonosulfate (**Figure 13b**). Wide linear ranges from 0.05 to 10.00 ng mL^{-1} and low LOD of 20 pg mL^{-1} (S/N = 3) were obtained, demonstrating the feasibility in practical clinical peroxymonosulfate detection (**Figure 13c**).

Electrochemiluminescence (ECL) is regarded as an effective and facile approach for the sensitive and selective detection of various biological analytes (Richter 2004). Zhu and coworkers developed an Fe–N–C SAC–luminol-O_2 ECL sensing platform to replace the traditional H_2O_2-luminol ECL system (**Figure 13d**) (Gu et al. 2020). The Fe–N–C SAzyme with unique OXD-like performance could serve as an advanced co-reactant accelerator to transform dissolved oxygen into ROS. The ECL intensity was noticeably enhanced in the O_2-saturated atmosphere (**Figure 13e**). On the contrary, there was weak luminescence in the N_2-saturated solution. As a result, this proposed Fe–N–C SAzyme–luminol ECL biosensing platform was applied for the evaluation of the antioxidant capacity in commercial beverages with satisfactory results. To gain deeper insights into the luminol-dissolved O_2-ECL mechanism, they fabricated two kinds of Ni SAzymes, Ni–N_4 (Ni–N_4/C) and Ni–N_2O_2 (Ni–N_2O_2/C), as co-reaction accelerators (**Figure 13f**) (Xie et al. 2021). By adjusting the coordination microenvironment of Ni-SACs, the electrochemical ORR behaviors of these two proof-of-concept Ni SAC models could be modulated. There was a four-electron mechanism on Ni–N_4/C to reduce O_2 to H_2O, while a two-electron process was more likely to generate H_2O_2 on the Ni–N_2O_2/C. The ECL performance of these two Ni SAC catalysts also presented different features: there was negligible ECL emission using the Ni–N_2O_2/C as the co-reaction accelerator. On the contrary, the introduction of Ni–N_4/C catalysts could efficiently improve the ECL intensity. Combined with the theoretical results, the Ni–N_4/C catalyst was shown to possess a lower energy barrier to activate oxygen molecules, which was more efficient in boosting the ECL reaction than Ni–N_2O_2/C. The feasibility of this Ni–N_4/C–O_2-luminol ECL system was further confirmed by the sensitive detection of the ascorbic acid (**Figure 13g**).

Other emerging types of biosensing methods and dual-modal biosensing platforms based on SAzymes have received extensive interest for achieving the ASSURED (affordable, sensitive, specific, user-friendly, rapid and robust, equipment-free, and deliverable to the end user) criteria defined by World Health Organization. For instance, a smart approach for the Fe SAzyme-based solution-gated graphene transistor (SGGT) was designed for real-time monitoring of Hg^{2+} ions in real water samples (**Figure 13h**) (Yao et al. 2020). The high signal amplification efficiency of this device was attributed to the introduction of Fe SAzymes. Wu's group also developed a Co-SAC-based SGGT device as a high-performance glucose sensor for

healthcare monitoring (Xiong et al. 2020). Furthermore, a Fe POD-like SAzyme anchored on aerogel was employed for a dual-function detection platform (**Figure 13i**) (Gao et al. 2021). This dual-function SAzyme-based biosensor exhibited excellent performance for the fluorescence and electrochemical detection of glucose.

5. Conclusions and Perspectives

Tracking back to the past few years, we have witnessed the flourishing development of SAzymes as one of the most active heterogeneous biocatalysts with excellent POD-like, OXD-like, and multiple enzyme-like performances. More importantly, the enzyme-like behavior of SAzymes is closely related to the local structure of the active metal center and its microenvironment. Up to now, a number of innovative and effective strategies have been developed to rationally design the targeted SAzymes, elucidate the underlying enzyme-catalytic mechanisms, and deepen the understanding of structure–property relationship, which have opened up diverse opportunities in the biosensing applications. Despite the breakthroughs accomplished so far in the field of SAzymes-based biosensing, there are still foreseeable challenges that await more collective and collaborative efforts for the advancement of SAzyme research (**Figure 14**).

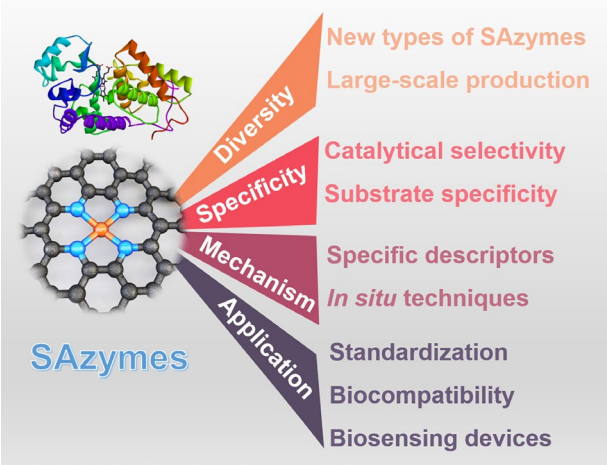

Figure 14. Schematic illustration of foreseeable challenges and future developments of SAzymes in biosensing application.

Firstly, new types of SAzymes with desired properties should be further explored. Most currently available SAzymes target to mimic redox enzymes. Other types of SAzymes such as hydrolase (Li et al. 2022b), transferase, lyase, isomerase, and ligase mimics could be

considered as new potential members of the SAzyme family. Although the reported number of SACs used in SAzymes has increased sharply, many are in the form of typical "transition metal SAC supported on N-doped carbon substrate (M–N–C)". It would be advantageous to explore diverse supports such as metallic oxide, metallic carbide, metallic hydroxide, and organic compounds that may offer another way of tuning the property of SAC sites. Also, new and green synthetic strategies for fabricating single-atom sites that allow high SAC density and maximum exposure are desired. Particularly, in order to meet the demand of practical biosensing applications, the large-scale and high-efficiency production of SAzymes should first be realized.

Secondly, the balance between the multi-enzyme mimicking activities and catalytic selectivity of SAzymes should be established at the atomic level. The unique advantages of maximum atom utilization and definite configuration have endowed SAzymes with high enzyme-like catalytical activities. However, the selectivity and specificity of SAzymes are still far behind natural enzymes under physiological conditions. Most SAzymes were reported to display at least two kinds of enzyme-like activities. Such multi-enzyme activities of SAzymes could be a double-edged sword for biosensing applications. On one hand, it would bring a revolutionary impact on biological cascade catalytic systems and pave the way for biomimetic cascade nanoreactors for a variety of biosensing applications. On the other hand, non-specific signals and undistinguishable side reactions could result due to the multi-enzyme-mimetic activities of SAzymes in complicated biocatalytic environments. To find out answers to this tricky question, the following aspects could be taken into consideration: (a) The enzyme-like reactions on SAzymes are also heterogeneous catalysis with multiple proton-coupled electron transfer processes. By regulating the coordination numbers, coordination atoms, and types of supports, the geometric and electronic configurations of SAzymes could be tailored to specifically target substrates.; (b) Theoretical calculations and machine learning could be of critical help in guiding the catalytic specificity of SAzymes. Some effective post-processing strategies, such as biorthogonal chemistry and molecularly imprinting, will also endow the SAzymes with tunable catalytic selectivity.; and (c) The hybridization of SAzymes with specific ligands (natural enzymes, aptamers, DNA, and antibodies) would construct biomimetic cascade catalytic biosensors that are specific for the desired substrates.

Thirdly, more research effort should be paid to the elucidation of the catalytic mechanism of SAzymes. The well-defined active sites of SACs have provided an ideal model to correlate local structures with various catalytic mechanisms. It is also highly desired to gain insight into the enzyme-like mechanism of SAzymes. Developing specific descriptors of SAzyme property would be very useful. The current works mostly focused on the influence of size, composition, morphology, and surface lattice on the catalytic performance of SAzymes (Wang et al. 2020). In addition to these surface factors, the inherent microenvironments of SAzymes, such as coordination configuration, d band center of metal site, e_g occupancy (Wang et al. 2019a), orbital coupling, adsorption (desorption) energy for intermediates, are also pivotal descriptors to reveal their potential enzyme-like activity and specificity. A general structure–property relationship is supposed to be understood and established based on those descriptors, which would provide a solid guide for the development of targeted SAzymes. For a molecular-level understanding of catalytic mechanism, some advanced *in situ/operando* techniques could be valuable tools. For instance, *in situ* X-ray diffraction (XRD), *in situ* scanning tunneling microscopy (STM) (Zheng and Lee 2022), *in situ* UV–vis spectroscopy, *in situ* Raman spectroscopy, *in situ* infrared spectroscopy (IR), *in situ* electron paramagnetic resonance (EPR), *in situ* mass spectroscopy (MS), and *in situ* X-ray absorption spectroscopy (XAS) (Chen et al. 2022) can offer real-time and *in situ* monitoring methods for the actual condition of SAzymes during the dynamic enzyme-like catalytical processes at the atomic level.

Fourthly, the standardization of catalytic activity unit would facilitate communication within the SAzyme community, as well as with other catalysis communities. Usually, the molar concentration or mass of nanozymes is used as the nanozyme unit (Zandieh and Liu 2022). For SAzymes, the molar concentration of single-atom active sites can also be used for quantifying the activity of SAzymes. Alternatively, by taking the real catalytically active site into consideration, the turnover rate (k_{cat}) can also be employed as an evaluation index for the enzyme-like performance (Zandieh and Liu 2021). Recently, Yan and coworkers have developed a standardized assay for the quantitative determination of the POD-like activity and kinetics (Jiang et al. 2018). The development of an accurate method of activity evaluation for more types of enzyme reactions is recommended.

Last but not least, the way to expand the application of SAzymes in innovative biosensing applications should be considered. For this, it is crucial to improve the biocompatibility of SAzymes. In addition to activity and specificity, water solubility and biotoxicity are also essential for promoting the practical implementation of SAzymes in the biosensing field. By combining surface engineering approaches with a controllable synthetic strategy of various SAzymes, it is anticipated that the biocompatibility of SAzymes could be dramatically improved. Also, innovative biosensing platforms should be invented to specifically tailor the various sensing mechanism of SAzymes to achieve precise target recognition with satisfactory accuracy and selectivity. The implementation of SAzymes in available biosensing devices and products is also of great value. For instance, Wu's group has incorporated personal protective equipment (PPE) with Cu oxidase-like SAzymes (Jin et al. 2022). The SAzymes are expected to offer enormous potential in the development of advanced portable and smart biosensing equipment in the near future.

In conclusion, the field of SAzymes is still in its developing stage. The fundamental understanding of enzyme-like catalytic mechanisms and the currently unsatisfactory specificity of SAzymes are the two major bottlenecks that need immediate attention. The most promising pathway is to precisely construct and modulate the atomic structure of SAzymes to reveal and control the reaction mechanisms. We hope this review can inspire future endeavors in SAzyme research and help develop the next-generation nanozymes.

Declaration of competing interest

The authors declare that they have no known competing financial interests or personal relationships that could have appeared to influence the work reported in this paper.

CRediT authorship contribution statement

Ying Wang: Investigation, Writing–original draft, Preparation. **Ruolan Du:** Investigation, Validation. **Lawrence Yoon Suk Lee:** Conceptualization, Writing–review & editing, Funding acquisition. **Kwok-Yin Wong:** Project administration, Funding acquisition.

Acknowledgements

We acknowledge the support from the Innovation and Technology Commission and The Hong Kong Polytechnic University. L.Y.S. Lee acknowledges the support from the Research Institute for Smart Energy of the Hong Kong Polytechnic University (Q-CDA3) and Research Grants Council of the Hong Kong SAR (PolyU15217521). K.-Y. Wong acknowledges the support from the Patrick S. C. Poon Endowed Professorship. Y.Wang acknowledges the support of the Postdoctoral Fellowships Scheme from the Hong Kong Polytechnic University (1-W189).

ORCID

Lawrence Yoon Suk Lee: 0000-0002-6119-4780

Kwok-Yin Wong: 0000-0003-4984-7109

References

Baddiley, J., Thain, E.M., Novelli, G.D., Lipmann, F., 1953. Nature 171 (4341), 76-76.
Bell, E.L., Finnigan, W., France, S.P., Green, A.P., Hayes, M.A., Hepworth, L.J., Lovelock, S.L., Niikura, H., Osuna, S., Romero, E., Ryan, K.S., Turner, N.J., Flitsch, S.L., 2021. Nature Reviews Methods Primers 1 (1), 1-46.
Berglund, G.I., Carlsson, G.H., Smith, A.T., Szöke, H., Henriksen, A., Hajdu, J., 2002. Nature 417 (6887), 463-468.
Bornscheuer, U.T., Huisman, G.W., Kazlauskas, R.J., Lutz, S., Moore, J.C., Robins, K., 2012. Nature 485 (7397), 185-194.
Breslow, R., 1995. Acc. Chem. Res. 28 (3), 146-153.
Bringas, M., Petruk, A.A., Estrin, D.A., Capece, L., Martí, M.A., 2017. Scientific Reports 7 (1), 10926.
Cai, X., Jiao, L., Yan, H., Wu, Y., Gu, W., Du, D., Lin, Y., Zhu, C., 2021. Mater. Today 44, 211-228.
Cao, F., Zhang, L., You, Y., Zheng, L., Ren, J., Qu, X., 2020. Angew. Chem. Int. Ed. 59 (13), 5108-5115.
Cao, S., Zhao, Z., Zheng, Y., Wu, Z., Ma, T., Zhu, B., Yang, C., Xiang, X., Ma, L., Han, X., Wang, Y., Guo, Q., Qiu, L., Cheng, C., 2022. Adv. Mater. 34 (16), 2200255.
Chang, B., Zhang, L., Wu, S., Sun, Z., Cheng, Z., 2022. Chemical Society Reviews 51 (9), 3688-3734.
Chang, M., Hou, Z., Wang, M., Yang, C., Wang, R., Li, F., Liu, D., Peng, T., Li, C., Lin, J., 2021. Angew. Chem. Int. Ed. 60 (23), 12971-12979.
Chen, H.-Q., Zou, L., Wei, D.-Y., Zheng, L.-L., Wu, Y.-F., Zhang, H., Li, J.-F., 2022. Chinese Journal of Catalysis 43 (1), 33-46.
Chen, M., Zhou, H., Liu, X., Yuan, T., Wang, W., Zhao, C., Zhao, Y., Zhou, F., Wang, X., Xue, Z., Yao, T., Xiong, C., Wu, Y., 2020. Small 16 (31), 2002343.
Chen, Y., Jiao, L., Yan, H., Xu, W., Wu, Y., Zheng, L., Gu, W., Zhu, C., 2021a. Anal. Chem. 93 (36), 12353-12359.
Chen, Y., Wang, P., Hao, H., Hong, J., Li, H., Ji, S., Li, A., Gao, R., Dong, J., Han, X., Liang, M., Wang, D., Li, Y., 2021b. Journal of the American Chemical Society 143 (44), 18643-18651.
Cheng, N., Li, J.-C., Liu, D., Lin, Y., Du, D., 2019. Small 15 (48), 1901485.
Chong, Y., Liu, Q., Ge, C., 2021. Nano Today 37, 1-16.
Cui, X., Li, W., Ryabchuk, P., Junge, K., Beller, M., 2018. Nat. Catal. 1 (6), 385-397.
Feng, M., Zhang, Q., Chen, X., Deng, D., Xie, X., Yang, X., 2022. Biosens. Bioelectron. 210, 114294.
Gallarati, S., Dingwall, P., Fuentes, J.A., Bühl, M., Clarke, M.L., 2020. Organometallics 39 (24), 4544-4556.
Gao, L., Zhuang, J., Nie, L., Zhang, J., Zhang, Y., Gu, N., Wang, T., Feng, J., Yang, D., Perrett, S., Yan, X., 2007. Nat. Nanotechnol. 2 (9), 577-583.
Gao, X., Ma, W., Mao, J., He, C.-T., Ji, W., Chen, Z., Chen, W., Wu, W., Yu, P., Mao, L., 2021. Chem. Sci. 12 (45), 15045-15053.
Gu, W., Wang, H., Jiao, L., Wu, Y., Chen, Y., Hu, L., Gong, J., Du, D., Zhu, C., 2020. Angew. Chem. Int. Ed. 59 (9), 3534-3538.
Hou, H., Mao, J., Han, Y., Wu, F., Zhang, M., Wang, D., Mao, L., Li, Y., 2019. Sci. China Chem. 62 (12), 1720-1724.
Huang, L., Chen, J., Gan, L., Wang, J., Dong, S., 2019a. Sci. Adv. 5 (5), 1-9.
Huang, Y., Ren, J., Qu, X., 2019b. Chem. Rev. 119 (6), 4357-4412.
Huo, M., Wang, L., Wang, Y., Chen, Y., Shi, J., 2019. ACS Nano 13 (2), 2643-2653.
Ji, S., Chen, Y., Wang, X., Zhang, Z., Wang, D., Li, Y., 2020. Chem. Rev. 120 (21), 11900-11955.
Ji, S., Jiang, B., Hao, H., Chen, Y., Dong, J., Mao, Y., Zhang, Z., Gao, R., Chen, W., Zhang, R., Liang, Q., Li, H., Liu, S., Wang, Y., Zhang, Q., Gu, L., Duan, D., Liang, M., Wang, D., Yan, X., Li, Y., 2021. Nat. Catal. 4 (5), 407-417.
Jiang, B., Duan, D., Gao, L., Zhou, M., Fan, K., Tang, Y., Xi, J., Bi, Y., Tong, Z., Gao, G.F., Xie, N., Tang, A., Nie, G., Liang, M., Yan, X., 2018. Nature Protocols 13 (7), 1506-1520.
Jiang, D., Ni, D., Rosenkrans, Z.T., Huang, P., Yan, X., Cai, W., 2019. Chem. Soc. Rev. 48 (14), 3683-3704.
Jiao, L., Kang, Y., Chen, Y., Wu, N., Wu, Y., Xu, W., Wei, X., Wang, H., Gu, W., Zheng, L., Song, W., Zhu, C., 2021. Nano Today 40, 101261.
Jiao, L., Wu, J., Zhong, H., Zhang, Y., Xu, W., Wu, Y., Chen, Y., Yan, H., Zhang, Q., Gu, W., Gu, L., Beckman, S.P., Huang, L., Zhu, C., 2020a. ACS Catal. 10 (11), 6422-6429.
Jiao, L., Xu, W., Yan, H., Wu, Y., Liu, C., Du, D., Lin, Y., Zhu, C., 2019. Analytical Chemistry 91 (18), 11994-11999.
Jiao, L., Xu, W., Zhang, Y., Wu, Y., Gu, W., Ge, X., Chen, B., Zhu, C., Guo, S., 2020b. Nano Today 35,

100971.
Jiao, L., Yan, H., Wu, Y., Gu, W., Zhu, C., Du, D., Lin, Y., 2020c. Angew. Chem. Int. Ed. 59 (7), 2565-2576.
Jiao, L., Ye, W., Kang, Y., Zhang, Y., Xu, W., Wu, Y., Gu, W., Song, W., Xiong, Y., Zhu, C., 2022. Nano Res. 15 (2), 959-964.
Jin, X., Gao, F., Qin, M., Yu, Y., Zhao, Y., Shao, T., Chen, C., Zhang, W., Xie, B., Xiong, Y., Yang, L., Wu, Y., 2022. ACS Nano 16 (5), 7755-7771.
Kaiser, S.K., Chen, Z., Faust Akl, D., Mitchell, S., Pérez-Ramírez, J., 2020. Chem. Rev. 120 (21), 11703-11809.
Kandathil, V., Patil, S.A., 2021. Advances in Colloid and Interface Science 294, 102485.
Kim, M.S., Lee, J., Kim, H.S., Cho, A., Shim, K.H., Le, T.N., An, S.S.A., Han, J.W., Kim, M.I., Lee, J., 2019. Adv. Funct. Mater. 30 (1), 1905410.
Krainer, F.W., Glieder, A., 2015. Applied Microbiology and Biotechnology 99 (4), 1611-1625.
Li, L., Chang, X., Lin, X., Zhao, Z., Gong, J., 2020a. Chemical Society Reviews 49 (22), 8156-8178.
Li, R., He, X., Javed, R., Cai, J., Cao, H., Liu, X., Chen, Q., Ye, D., Zhao, H., 2022a. Sci. Total Environ. 834, 155428.
Li, S., Zhou, Z., Tie, Z., Wang, B., Ye, M., Du, L., Cui, R., Liu, W., Wan, C., Liu, Q., Zhao, S., Wang, Q., Zhang, Y., Zhang, S., Zhang, H., Du, Y., Wei, H., 2022b. Nature Communications 13 (1), 827.
Li, X., Liu, L., Ren, X., Gao, J., Huang, Y., Liu, B., 2020b. Sci. Adv. 6 (39), 1-19.
Li, Z., Liu, F., Jiang, Y., Ni, P., Zhang, C., Wang, B., Chen, C., Lu, Y., 2022c. Nano Res. 15 (5), 4411-4420.
Lu, X., Gao, S., Lin, H., Tian, H., Xu, D., Shi, J., 2022. Natl. Sci. Rev., 1-30.
Luo, X., Luo, Z., Wei, X., Jiao, L., Fang, Q., Wang, H., Wang, J., Gu, W., Hu, L., Zhu, C., 2022. Anal. Chem. 94 (2), 1390-1396.
Lyu, Z., Ding, S., Wang, M., Pan, X., Feng, Z., Tian, H., Zhu, C., Du, D., Lin, Y., 2021. Nano-Micro Lett. 13 (1), 146.
Ma, C.-B., Xu, Y., Wu, L., Wang, Q., Zheng, J.-J., Ren, G., Wang, X., Gao, X., Zhou, M., Wang, M., Wei, H., 2022. Angew. Chem. Int. Ed., 1-10.
Ma, W., Mao, J., Yang, X., Pan, C., Chen, W., Wang, M., Yu, P., Mao, L., Li, Y., 2019. Chem. Commun. 55 (2), 159-162.
Manea, F., Houillon, F.B., Pasquato, L., Scrimin, P., 2004. Angew. Chem. Int. Ed. 43 (45), 6165-6169.
Muhammad, P., Hanif, S., Li, J., Guller, A., Rehman, F.U., Ismail, M., Zhang, D., Yan, X., Fan, K., Shi, B., 2022. Nano Today 45, 101530.
Ouyang, H., Zhang, L., Jiang, S., Wang, W., Zhu, C., Fu, Z., 2020. Chem. Eur. J. 26 (34), 7583-7588.
Pei, J., Zhao, R., Mu, X., Wang, J., Liu, C., Zhang, X.-D., 2020. Biomater. Sci. 8 (23), 6428-6441.
Qiao, B., Wang, A., Yang, X., Allard, L.F., Jiang, Z., Cui, Y., Liu, J., Li, J., Zhang, T., 2011. Nat. Chem. 3 (8), 634-641.
Qin, Y., Wen, J., Wang, X., Jiao, L., Wei, X., Wang, H., Li, J., Liu, M., Zheng, L., Hu, L., Gu, W., Zhu, C., 2022. ACS Nano 16 (2), 2997-3007.
Qin, Y., Wen, J., Zheng, L., Yan, H., Jiao, L., Wang, X., Cai, X., Wu, Y., Chen, G., Chen, L., Hu, L., Gu, W., Zhu, C., 2021. Nano Lett. 21 (4), 1879-1887.
Richter, M.M., 2004. Chemical Reviews 104 (6), 3003-3036.
Shen, L., Khan, M.A., Wu, X., Cai, J., Lu, T., Ning, T., Liu, Z., Lu, W., Ye, D., Zhao, H., Zhang, J., 2022. Biosensors and Bioelectronics 205, 114097.
Song, G., Zhang, J., Huang, H., Wang, X., He, X., Luo, Y., Li, J.-c., Huang, K., Cheng, N., 2022. Food Chem. 387, 132896.
Sun, L., Yan, Y., Chen, S., Zhou, Z., Tao, W., Li, C., Feng, Y., Wang, F., 2022. Anal. Bioanal. Chem. 414 (5), 1857-1865.
Tian, R., Ma, H., Ye, W., Li, Y., Wang, S., Zhang, Z., Liu, S., Zang, M., Hou, J., Xu, J., Luo, Q., Sun, H., Bai, F., Yang, Y., Liu, J., 2022. Advanced Functional Materials, 2204025.
Wang, A., Li, J., Zhang, T., 2018. Nat. Rev. Chem. 2 (6), 65-81.
Wang, D., Wu, H., Wang, C., Gu, L., Chen, H., Jana, D., Feng, L., Liu, J., Wang, X., Xu, P., Guo, Z., Chen, Q., Zhao, Y., 2021a. Angew. Chem. Int. Ed. 60 (6), 3001-3007.
Wang, D., Zhao, Y., 2021. Chem 7 (10), 2635-2671.
Wang, J., Zhong, W., Liu, X., Yang, T., Li, F., Li, Q., Cheng, W., Gao, C., Jiang, Z., Jiang, J., Cui, H., 2017a. Anal. Chem. 89 (24), 13518-13523.
Wang, S., Cazelles, R., Liao, W.-C., Vázquez-González, M., Zoabi, A., Abu-Reziq, R., Willner, I., 2017b. Nano Lett. 17 (3), 2043-2048.
Wang, S., Hu, Z., Wei, Q., Cui, P., Zhang, H., Tang, W., Sun, Y., Duan, H., Dai, Z., Liu, Q., Zheng, X., 2022a.

ACS Appl. Mater. Interfaces 14 (18), 20669-20681.
Wang, S., Hu, Z., Wei, Q., Zhang, H., Tang, W., Sun, Y., Duan, H., Dai, Z., Liu, Q., Zheng, X., 2022b. Nano Res. 15 (5), 4266-4273.
Wang, W., Zhu, Y., Zhu, X., Zhao, Y., Xue, Z., Xiong, C., Wang, Z., Qu, Y., Cheng, J., Chen, M., Liu, M., Zhou, F., Zhang, H., Jiang, Z., Hu, Y., Zhou, H., Wang, H., Li, Y., Liu, Y., Wu, Y., 2021b. ACS Appl. Mater. Interfaces 13 (38), 45269-45278.
Wang, X., Gao, X.J., Qin, L., Wang, C., Song, L., Zhou, Y.-N., Zhu, G., Cao, W., Lin, S., Zhou, L., Wang, K., Zhang, H., Jin, Z., Wang, P., Gao, X., Wei, H., 2019a. Nature Communications 10 (1), 704.
Wang, X., Shi, Q., Zha, Z., Zhu, D., Zheng, L., Shi, L., Wei, X., Lian, L., Wu, K., Cheng, L., 2021c. Bioact. Mater. 6 (12), 4389-4401.
Wang, Y., Cui, X., Zhao, J., Jia, G., Gu, L., Zhang, Q., Meng, L., Shi, Z., Zheng, L., Wang, C., Zhang, Z., Zheng, W., 2019b. ACS Catalysis 9 (1), 336-344.
Wang, Y., Huang, R., Han, J.W., 2022c. Journal of Physics D: Applied Physics 55 (32), 323001.
Wang, Y., Jia, G., Cui, X., Zhao, X., Zhang, Q., Gu, L., Zheng, L., Li, L.H., Wu, Q., Singh, D.J., Matsumura, D., Tsuji, T., Cui, Y.-T., Zhao, J., Zheng, W., 2021d. Chem 7 (2), 436-449.
Wang, Y., Park, B.J., Paidi, V.K., Huang, R., Lee, Y., Noh, K.-J., Lee, K.-S., Han, J.W., 2022d. ACS Energy Letters 7 (2), 640-649.
Wang, Y., Qi, K., Yu, S., Jia, G., Cheng, Z., Zheng, L., Wu, Q., Bao, Q., Wang, Q., Zhao, J., Cui, X., Zheng, W., 2019c. Nano-Micro Lett. 11 (1), 1-13.
Wang, Y., Zhang, Z., Jia, G., Zheng, L., Zhao, J., Cui, X., 2019d. Chem. Commun. 55 (36), 5271-5274.
Wang, Z., Zhang, R., Yan, X., Fan, K., 2020. Mater. Today 41, 81-119.
Wei, H., Wang, E., 2013. Chem. Soc. Rev. 42 (14), 6060-6093.
Wei, X., Song, S., Song, W., Xu, W., Jiao, L., Luo, X., Wu, N., Yan, H., Wang, X., Gu, W., Zheng, L., Zhu, C., 2021. Anal. Chem. 93 (12), 5334-5342.
Williams, P.A., Cosme, J., Ward, A., Angove, H.C., Matak Vinković, D., Jhoti, H., 2003. Nature 424 (6947), 464-468.
Wu, W., Huang, L., Wang, E., Dong, S., 2020a. Chem. Sci. 11 (36), 9741-9756.
Wu, X., Sun, Y., He, T., Zhang, Y., Zhang, G.-J., Liu, Q., Chen, S., 2021. Langmuir 37 (38), 11309-11315.
Wu, Y., Wu, J., Jiao, L., Xu, W., Wang, H., Wei, X., Gu, W., Ren, G., Zhang, N., Zhang, Q., Huang, L., Gu, L., Zhu, C., 2020b. Anal. Chem. 92 (4), 3373-3379.
Wu, Z., Wang, C., Luo, Z., Qin, Y., Wang, X., Wen, J., Hu, L., Gu, W., Zhu, C., 2022. Anal. Chem. 94 (18), 6866-6873.
Xi, J., Zhang, R., Wang, L., Xu, W., Liang, Q., Li, J., Jiang, J., Yang, Y., Yan, X., Fan, K., Gao, L., 2021. Adv. Funct. Mater. 31 (9), 2007130.
Xiang, H., Feng, W., Chen, Y., 2020. Advanced Materials 32 (8), 1905994.
Xie, X., Wang, D.P., Guo, C., Liu, Y., Rao, Q., Lou, F., Li, Q., Dong, Y., Li, Q., Yang, H.B., Hu, F.X., 2021. Anal. Chem. 93 (11), 4916-4923.
Xiong, C., Tian, L., Xiao, C., Xue, Z., Zhou, F., Zhou, H., Zhao, Y., Chen, M., Wang, Q., Qu, Y., Hu, Y., Wang, W., Zhang, Y., Zhou, X., Wang, Z., Yin, P., Mao, Y., Yu, Z.-Q., Cao, Y., Duan, X., Zheng, L., Wu, Y., 2020. Sci. Bull. 65 (24), 2100-2106.
Xu, B., Li, S., Zheng, L., Liu, Y., Han, A., Zhang, J., Huang, Z., Xie, H., Fan, K., Gao, L., Liu, H., 2022. Adv. Mater. 34 (15), 2107088.
Xu, B., Wang, H., Wang, W., Gao, L., Li, S., Pan, X., Wang, H., Yang, H., Meng, X., Wu, Q., Zheng, L., Chen, S., Shi, X., Fan, K., Yan, X., Liu, H., 2019. Angew. Chem. Int. Ed. 58 (15), 4911-4916.
Xu, Q., Hua, Y., Zhang, Y., Lv, M., Wang, H., Pi, Y., Xie, J., Wang, C., Yong, Y., 2021. Adv. Healthc. Mater. 10 (22), 2101374.
Xu, W., Kang, Y., Jiao, L., Wu, Y., Yan, H., Li, J., Gu, W., Song, W., Zhu, C., 2020. Nano-Micro Lett. 12 (1), 184.
Yan, R., Sun, S., Yang, J., Long, W., Wang, J., Mu, X., Li, Q., Hao, W., Zhang, S., Liu, H., Gao, Y., Ouyang, L., Chen, J., Liu, S., Zhang, X.-D., Ming, D., 2019. ACS Nano 13 (10), 11552-11560.
Yang, J., Zhang, R., Zhao, H., Qi, H., Li, J., Li, J.-F., Zhou, X., Wang, A., Fan, K., Yan, X., Zhang, T., 2022. Exploration n/a (n/a), 20210267.
Yang, W., Yang, X., Zhu, L., Chu, H., Li, X., Xu, W., 2021. Coord. Chem. Rev 448, 214170.
Yang, X.-F., Wang, A., Qiao, B., Li, J., Liu, J., Zhang, T., 2013. Acc. Chem. Res. 46 (8), 1740-1748.
Yao, L., Gao, S., Liu, S., Bi, Y., Wang, R., Qu, H., Wu, Y., Mao, Y., Zheng, L., 2020. ACS Appl. Mater. Interfaces 12 (5), 6268-6275.
Zandieh, M., Liu, J., 2021. ACS Nano 15 (10), 15645-15655.

Zandieh, M., Liu, J., 2022. Langmuir 38 (12), 3617-3622.
Zhang, C., Chen, C., Zhao, D., Kang, G., Liu, F., Yang, F., Lu, Y., Sun, J., 2022a. Anal. Chem. 94 (8), 3485-3493.
Zhang, H., Lu, X.F., Wu, Z.-P., Lou, X.W.D., 2020. ACS Central Science 6 (8), 1288-1301.
Zhang, R., Yan, X., Fan, K., 2021a. Acc. Mater. Res 2 (7), 534-547.
Zhang, W., Chao, Y., Zhang, W., Zhou, J., Lv, F., Wang, K., Lin, F., Luo, H., Li, J., Tong, M., Wang, E., Guo, S., 2021b. Advanced Materials 33 (36), 2102576.
Zhang, X., Li, G., Chen, G., Wu, D., Wu, Y., James, T.D., 2021c. Adv. Funct. Mater. 31 (50), 2106139.
Zhang, X., Zhang, M., Deng, Y., Xu, M., Artiglia, L., Wen, W., Gao, R., Chen, B., Yao, S., Zhang, X., Peng, M., Yan, J., Li, A., Jiang, Z., Gao, X., Cao, S., Yang, C., Kropf, A.J., Shi, J., Xie, J., Bi, M., van Bokhoven, J.A., Li, Y.-W., Wen, X., Flytzani-Stephanopoulos, M., Shi, C., Zhou, W., Ma, D., 2021d. Nature 589 (7842), 396-401.
Zhang, Y., Yang, J., Ge, R., Zhang, J., Cairney, J.M., Li, Y., Zhu, M., Li, S., Li, W., 2022b. Coordination Chemistry Reviews 461, 214493.
Zhao, C., Xiong, C., Liu, X., Qiao, M., Li, Z., Yuan, T., Wang, J., Qu, Y., Wang, X., Zhou, F., Xu, Q., Wang, S., Chen, M., Wang, W., Li, Y., Yao, T., Wu, Y., Li, Y., 2019. Chem. Commun. 55 (16), 2285-2288.
Zheng, W., Lee, L.Y.S., 2022. Chemistry-An Asian Journal, e202200384.
Zhou, M., Jiang, Y., Wang, G., Wu, W., Chen, W., Yu, P., Lin, Y., Mao, J., Mao, L., 2020. Nat. Commun. 11 (1), 3188.
Zhu, Y., Wang, W., Cheng, J., Qu, Y., Dai, Y., Liu, M., Yu, J., Wang, C., Wang, H., Wang, S., Zhao, C., Wu, Y., Liu, Y., 2021. Angew. Chem. Int. Ed. 60 (17), 9480-9488.